



A regime shift in the interhemispheric teleconnection between the Yellow and East China Seas and the southeastern tropical Pacific during the boreal summer

Yong Sun Kim^{1,2} · Minho Kwon^{1,2} · Eui-Seok Chung³ · Sang-Wook Yeh⁴ · Jin-Yong Jeong⁵ · Chan Joo Jang^{1,6}

Received: 1 October 2021 / Accepted: 26 September 2022 / Published online: 20 October 2022
© The Author(s), under exclusive licence to Springer-Verlag GmbH Germany, part of Springer Nature 2022

Abstract

A drastic regime shift is observed in the early summer connection between the Yellow and East China Seas (YECS) and the tropical Pacific in the early 2000s through statistical estimations on reconstructed datasets for the period 1982–2020. During the pre-2003 period, prior to the regime shift, the summer sea surface temperatures (SSTs) in the YECS were modulated by local oceanic and atmospheric processes, along with their marginal coupling to the tropical Pacific. In contrast, an interhemispheric coupling emerges between the YECS and southeastern tropical Pacific after the regime shift. This teleconnection is attributed to a reduced El Niño signature in the tropical Pacific, which favors the emergence of the South Pacific meridional mode (SPMM) independently from the El Niño–Southern Oscillation signals. The SPMM-related SST anomalies invoke changes in rainfall and vertical motion over the western tropical Pacific, activating the western North Pacific subtropical high over the Philippine Sea. This atmospheric circulation system acts as an atmospheric bridge to mediate the air-sea interacted variability associated with the SPMM into the YECS. The susceptibility of the YECS to atmospheric forcing highlights the role of SST in the YECS as a potential indicator of global-scale climate change.

Keywords South Pacific Meridional Mode · El Niño–Southern Oscillation · East Asian Summer Monsoon · Western North Pacific subtropical high · La Niña-like mean state

1 Introduction

The Yellow and East China Seas (YECS; Fig. 1a) comprise a well-developed continental shelf supporting a large, productive marine ecosystem in the northwestern Pacific

marginal seas (Beardsley et al. 1985; Fan and Huang 2008; Belkin 2009). The YECS have undergone substantial long-term changes in their physical and ecological environments over the last few decades (Belkin 2009; Yeh and Kim 2010; Bao and Ren 2014; Liao et al. 2015; Cai et al. 2017; Kim et al. 2022). Research on climate changes in the YECS has focused on winter sea surface temperature (SST), which represents a primary mode of long-term variability along with the recognition of a remarkable trend during the last few decades (Yeh and Kim 2010; Zhang et al. 2010; Bao and Ren 2014; Cai et al. 2017). Meridional wind anomalies determine water temperature by modulating air-sea turbulent heat fluxes in winter when the water column is fully mixed (Yeh and Kim 2010; Cai et al. 2017; Kim et al. 2018a, b). This wind-driven basin-scale temperature change is locally compensated by oceanic heat advection associated with upwind currents over the central trough (Lie and Cho 2016; Tak et al. 2016; Kim et al. 2018a).

Less is known about a mechanism for summer SST variability, even though its variance is several times greater than that for the winter SST in the YECS (Supplementary Fig.

✉ Chan Joo Jang
cjjang@kiost.ac.kr

¹ Ocean Circulation Research Center, Korea Institute of Ocean Science and Technology, Busan 49111, South Korea

² Ocean Science and Technology School, Korea Maritime and Ocean University, Busan 49112, South Korea

³ Division of Atmospheric Sciences, Korea Polar Research Institute, Incheon 21990, South Korea

⁴ Department of Marine Sciences and Convergent Technology, Hanyang University, ERICA, Ansan 15588, South Korea

⁵ Marine Disaster Research Center, Korea Institute of Ocean Science and Technology, Busan 49111, South Korea

⁶ Department of Integrated Ocean Sciences, University of Science and Technology, Daejeon 34113, South Korea

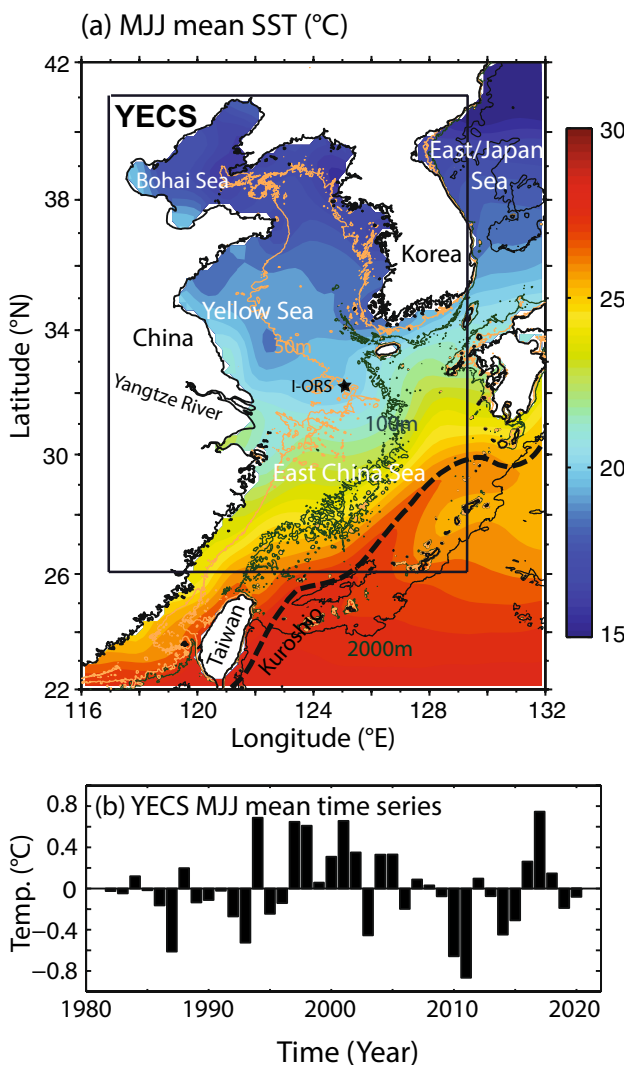


Fig. 1 **a** The spatial distribution of the early summer (MJJ) mean SST (shading, °C) for the period 1982–2020, and **b** its time series averaged over the Yellow and East China Seas (YECS; 117° E–129.5° E/26° N–41° N), defined as the YECS summer SST index. The thin contours in (a) are the 50 m (tan), 100 m (blue), and 2000 m (black) isobaths. The thick dashed line is the 1.15 m sea surface height to represent the mean path of the Kuroshio, following Wang and Oey (2014). The black star in the central YECS represents the Ieodo Ocean Research Station (I-ORS)

S1a). The lack of literature on this topic is partially due to the complexity of factors controlling summer SSTs in comparison to those for winter SSTs. These factors include southerly winds associated with large-scale atmospheric circulation (Zhang et al. 2010; Liu et al. 2013; Cai et al. 2017) and local features such as intense summer rainfall (Yang and Lau 2004; Ha et al. 2012; Fan et al. 2013) and the accompanying runoff from adjacent rivers (Belkin 2009; Park et al. 2011), frequent tropical cyclones (Du et al. 2011; Park et al. 2019), and non-local climate modes including El Niño (Park and Oh 2000; Wang et al. 2000; Liu et al. 2013) and Atlantic

multidecadal oscillation (AMO; Zhang et al. 2010). In addition, intrinsic processes associated with mixed layer depth, strength of stratification, and turbulent tidal mixing partially contribute to SST evolution (Kim et al. 2022).

A key process known to regulate local winds, precipitation, and typhoons, thereby determining the amplitude of the East Asian summer monsoon (EASM; Ha et al. 2012) and summer SST over the YECS, is the western North Pacific subtropical high (WNPSH; Wang et al. 2000, 2013; Yang and Lau 2004; Yim et al. 2008; Du et al. 2011; Fan et al. 2013; Liu et al. 2013; Xiang et al. 2013; Xie et al. 2016; Cai et al. 2017). The anomalous WNPSH could be triggered by a cold sea surface anomaly after the mature phase of the equatorial Pacific warming (i.e., El Niño) during the boreal winter months (Wang et al. 2000). Thus, literature has postulated a causal relationship between El Niño and the summer SSTs in the YECS with a lag of several months (Park and Oh 2000; Liu et al. 2013; Wu et al. 2016). However, the reported correlations were generally low, and the El Niño–Southern Oscillation (ENSO) region, which could act as a forcing region to modulate the EASM, was inconsistent in the literature. Wu et al. (2016), for instance, demonstrated that after removing long-term trends and annual cycles in the YECS, SST anomalies rendered a correlation coefficient of 0.31 with the 6-month preceding Nino3 SST index (SST anomaly averaged over 5° S–5° N, 150° W–90° W) from 1982 to 2011. Liu et al. (2013) demonstrated that the China Seas warmed approximately 4–10 months after the equatorial Pacific SST anomalies reached their maximum. A power spectrum coherency analysis also showed that anomalous SSTs in the East Asian marginal seas (25° N–45° N, 117° E–141° E) varied coherently for the 5–9 months preceding Nino3.4 (5° S–5° N, 170° W–120° W) SST index, particularly in a 2–3-year frequency band for the period 1951–1996 (Park and Oh 2000). A few studies have pointed out the importance of cooling anomalies in the central equatorial Pacific (i.e., the Nino4 region) (5° S–5° N, 160° E–150° W) in strengthening the WNPSH, especially during the development phase of La Niña (Lau and Nath 1996; Fan et al. 2013; Wang et al. 2013).

This discrepancy in the literature on the relationship between the summer SST anomaly of the YECS and ENSO forcing regions could be a result of the shift in the El Niño type or the existence of ENSO precursors. First, the El Niño type is believed to have changed between the canonical eastern Pacific warming-type El Niño (EP El Niño) and the central Pacific warming-type El Niño (CP El Niño). In recent decades, the latter has occurred more frequently than the typical EP El Niño (e.g., Yeh et al. 2009, 2015; Di Lorenzo et al. 2010; Yeo et al. 2012; Xiang et al. 2013; Jo et al. 2015; Capotondi et al. 2015; Stuecker 2018) presumably because of global warming (Yeh et al. 2009; Yeo and Kim 2014) and its positive feedback with the North Pacific meridional mode

(Liguori and Di Lorenzo 2018; Stuecker 2018). A shift in the El Niño type triggers the resultant interactions between SSTs and atmospheric variables, consequently resulting in considerable changes in the extratropics (Deser and Phillips 2006; Yim et al. 2008; Di Lorenzo et al. 2015; Yeo and Kim 2014; Newman et al. 2016). This drastic basin-scale change, often summarized with the term ‘regime shift’ in the literature (Bond et al. 2003; Overland et al. 2008), possibly renders a marginal and insignificant relationship between the YECS and equatorial Pacific mentioned above. The second candidate accounting for this discrepancy is the existence of ENSO precursors: north/south Pacific meridional modes (Vimont et al. 2003; Chang et al. 2007; Zhang et al. 2014a, 2021; Min et al. 2017; You and Furtado 2017; Larson et al. 2018; Stuecker 2018). Approximately two or three seasons before an El Niño event reaches its mature phase, a weakening of the off-equatorial trade winds modulates latent heat fluxes, exciting warm SST anomalies along the western coast of North/South America (Vimont et al. 2003; Chang et al. 2007; Zhang et al. 2014a). These meridional mode-related temperature anomalies tend to extend toward the equatorial Pacific via the wind-evaporation-SST (WES) feedback and background current, then modulating precipitation around the inter-tropical convergence zone (ITCZ). Consequently, atmospheric responses are triggered, forming a tropic–extra-tropic connection (Trenberth et al. 1998; Wang et al. 2000; Deser et al. 2004; He et al. 2011; Zhang et al. 2014a; Wu et al. 2015). If these meridional modes directly impact the summer monsoon in the western North Pacific, the low correlations estimated from the YECS summer SST and ENSO SST indices in previous studies may be justifiable.

This study investigates the impact of the tropical Pacific teleconnection on the summer SSTs in the YECS by considering these two hypotheses. To elucidate the atmospheric bridge connecting the equatorial Pacific and the YECS, we characterized large-scale atmospheric circulation and precipitation anomalies associated with the year-to-year summer SST variance in the YECS. We compared the large-scale atmospheric and oceanic conditions in shaping summer SSTs in the YECS. The EP El Niño-like pattern seems to have modulated the EASM by forming wind anomalies through the WNPSH but left a marginal signal in the summer SSTs in the YECS before the early 2000s. In contrast, the South Pacific Meridional Mode (SPMM; Zhang et al. 2014a) determines the YECS summer SSTs after the early 2000s, when EP El Niño is relatively inactive. The remainder of this paper is structured to demonstrate how this drastic change occurred. Section 2 describes the observational and reanalysis datasets and analysis methods. Section 3 shows that a regime shift in teleconnection between these two regions occurred in the early 2000s. In Sect. 4, we discuss that this regime shift could be related to the equatorial Pacific’s mean state and possible dynamics of how the

atmospheric footprint associated with the SPMM emerges over the SSTs of the YECS. Section 5 provides the summary and conclusions.

2 Data and methods

This study mainly analyzed the optimum interpolation SST version 2 (OISSTv2) data from the National Oceanic and Atmospheric Administration (NOAA; Reynolds et al. 2007) for the 39-year period, from 1982 to 2020, with a spatial resolution of $1/4^\circ \times 1/4^\circ$. This dataset was optimally merged based on Advanced Very High-Resolution Radiometer (AVHRR) observations with ancillary in-situ measurements. Intercomparison studies have suggested that the OISSTv2 is consistent with surface drifters and other SST datasets, not only in open oceans (Reynolds and Chelton 2010) but also in coastal seas (Lima and Wethey 2012; Liao et al. 2015; see Fig. S1b, c) with the unique advantage of persistent quality over almost four decades. Considering the spatial coverage of the YECS (117° E– 129.5° E/ 26° N– 41° N) spanning 12.5° longitude by 15° latitude, the OISSTv2 might be a unique and pertinent dataset for the long-term study of SST variability within the YECS. Other reanalysis datasets with coarser resolutions, such as the Hadley Centre Ice and Sea Surface Temperature (HadISST; 1° horizontal resolution; Rayner et al. 2003) or the Extended Reconstructed Sea Surface Temperature (ERSSTv5; 2° resolution), do not alter our results, as discussed in Sect. 3.1. The domain does not fully cover the southern part of the East China Sea to exclude a local impact from the Kuroshio Current. In this study, both spring and summer refer to the boreal seasons.

We estimated monthly anomalies by subtracting the study period (1982–2020) means from each calendar month and a linear trend at each grid point. The average SST trend throughout the YECS was 0.22°C per decade, accounting for 26.5% of the total variance after removing the seasonal cycle. The early summer of May–June–July (MJJ) averaged fields were computed from the monthly anomalies to disengage a sub-seasonal perturbation associated with tropical cyclones. The genesis of the tropical cyclone and its activity over the western North Pacific tend to form a climatological peak in August and September as the cross-equatorial flows and monsoonal westerlies are fully developed (Wang and Zhou 2008; Choi and Ha 2018). Its movement leaves an impulsive, sub-seasonal signal on SSTs over the YECS (Park et al. 2019), hence blurring climatological SST variability.

This study employed primary statistical tools, including linear regression, correlation, and singular value decomposition (SVD, also known as maximum covariance analysis), to identify an atmospheric pattern that evolves coherently with the MJJ mean SST of the YECS. We defined the MJJ-SST anomalies averaged over the YECS as the YECS summer

SST index (Fig. 1b). This index is almost identical to the first mode of principal component (PC1) for the summer SST anomalies in the YECS. The correlation coefficient between this index and PC1 is 0.90, explaining approximately 51% of the total year-to-year SST variance of the YECS. The index is separated from higher modes according to North et al. (1982). To identify an atmospheric bridge, we analyzed the Climate Prediction Center (CPC) Merged Analysis of Precipitation (CMAP) data (Xie and Arkin 1997), as well as wind, geopotential height, and convective and large-scale precipitation fields from the fifth-generation European Centre for Medium-range Weather Forecasts (ECMWF) atmospheric reanalysis (ERA5) for the period 1982–2020 with a spatial resolution of 0.5° (Hersbach et al. 2020). For the statistical significance test, we estimated the p-value based on a two-tailed Student's t-test with an effective degree of freedom computed considering a lag-1 autocorrelation in the time series (Bretherton et al. 1999).

3 Results

3.1 Relationship between the YECS summer SST and the Pacific and Indian Ocean SSTs

Figure 2a shows the simultaneous correlation coefficients of the SST anomalies in the Pacific and Indian Oceans and the YECS summer SST index for the 39-year study period (1982–2020). The coefficients that are statistically

significant at the 90% confidence level are shown in Fig. 2a. Apparent correlations emerge in three regions: the mid-latitude of the northwest Pacific around the YECS, southeast tropical Pacific (SEP; 20° S–10° S/130° W–100° W, the red box in Fig. 2a) near South America, and southwest tropical Indian Ocean (SWI) east of Madagascar Island (25° S–17° S/35° E–60° E, the green box in Fig. 2a). While strong correlations around the YECS seem reasonable, those in the Southern Hemisphere are unexpected. The correlations for the SEP ($r=0.48$, $p < 0.01$) and SWI ($r=-0.37$, $p=0.018$) are significant at the 95% confidence level but somewhat weak. We plotted the time series of the YECS and the SEP/SWI-averaged SST anomalies together in Fig. 2b, which represents a contrast in the SST temporal evolution of the YECS and SEP/SWI regions before and after the early 2000s. The year-to-year fluctuation of the summer YECS SST anomalies (the black bars in Fig. 2b) is precisely in tune with those of the SEP (the red line) only during the post-2003 period ($r=0.74$, $p < 0.01$) but not during 1982–2002 ($r=0.19$, $p > 0.1$). Similarly, a negative correlation of -0.44 was estimated for the SWI only during 2003–2020.

The correlations estimated by applying a nine-year sliding window also render a robust YECS–SEP/SWI coupling only during the period after the 2000s (Fig. 2c). The correlation between the YECS and SEP SST anomalies in the sliding estimation increases to 0.94 around the early 2010s and then tends to decrease slightly in the last few years. Sliding correlations applied to the HadISST (Fig. S2), which spanned the period 1870–2020, are similar to

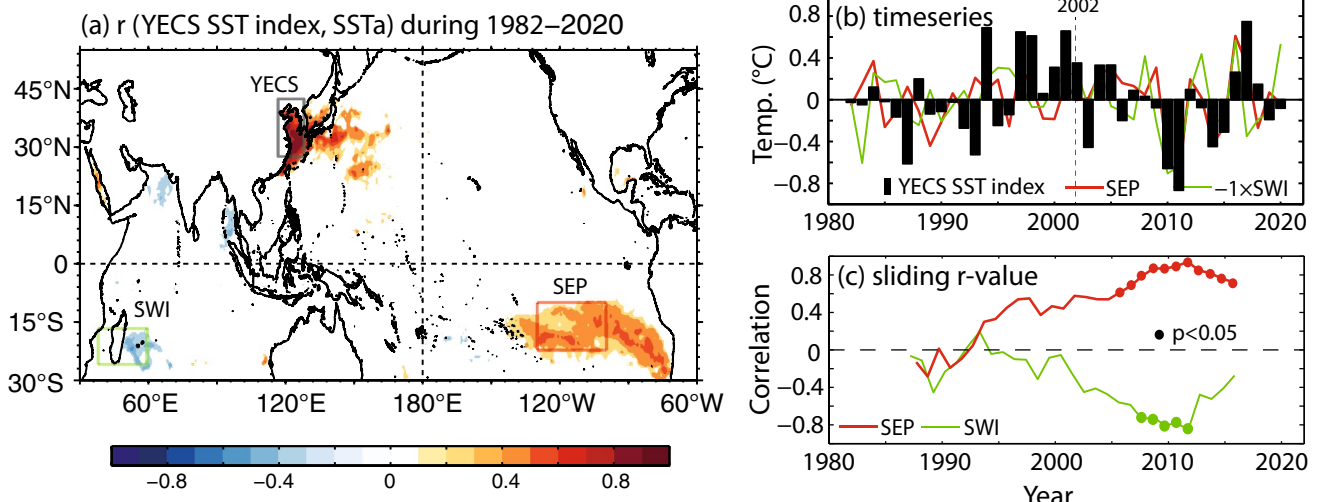


Fig. 2 **a** Map of the simultaneous correlation coefficients between the YECS summer SST index and SST anomalies in the Pacific and Indian Oceans during 1982–2020. The correlation coefficients above the 90% confidence level are shaded. **b** Time series of the YECS summer SST index (black bars) and SST anomalies averaged over the Southeastern Pacific (SEP; 130° E–100° W/20° S–10° S, red line) and over the Southwestern Indian (SWI; 35° E–60° E/25° S–17° S,

green line) oceans. In **b**, the $-1 \times$ SWI SST anomaly is plotted to show the inverse relationship between the MJJ mean SST anomalies of the YECS and the SWI. The nine-year moving correlation coefficients between the YECS summer SST index and the SEP and SWI SST anomalies are illustrated in **c**, with the central year of each moving period plotted on the x-axis. The dots represent the statistically significant correlations at the 95% confidence level

those shown in Fig. 2c which represents the significant correlations between the YECS and the SEP/SWI SST anomalies after the early 2000s. The ERSSTv5 with a coarser horizontal resolution of 2° also yields significant correlation coefficients, but only with the SEP SST for the period after the late 1990s. These results suggest the insensitivity of our finding: a regime shift in the early 2000s occurred in terms of the YECS–SEP teleconnection. Noteworthy is that the calculated correlations for the pre-satellite era are of questionable quality because of the lack of in-situ observations in both the YECS and SEP/SWI regions (Kim et al. 2018a; Zhang et al. 2014a, 2021).

Previous articles have suggested a lagged relationship between the equatorial Pacific SSTs and summer SSTs around the YECS. This study conducts a lead-lag cross-correlation analysis between the YECS summer SST index and the SST anomalies for the periods 1982–2002 (left column of Fig. 3) and 2003–2020 (right column of Fig. 3) with various time lags. On the contribution of the equatorial Pacific SSTs to the YECS summer SST variance, we failed to find a meaningful correlation in the eastern or central Pacific for any lagged months, both before and after the early 2000s. Insignificant correlations of less than ± 0.15 between the YECS summer SST index and the lead-lag ENSO indices for different regions—Nino3, Nino3.4, and Nino4—provide additional evidence for the ENSOs' marginal role in altering the summer YECS SSTs (Fig. S3). In addition, no significant relationship was found between the YECS summer SST index and either the Pacific decadal oscillation (PDO), a low-frequency modulation of the ENSO, or the AMO (Fig. S3), which has been mentioned in previous studies as a key index for modulating low-frequency SST variability in the YECS (Zhang et al. 2010; Liao et al. 2015; Kim et al. 2018a).

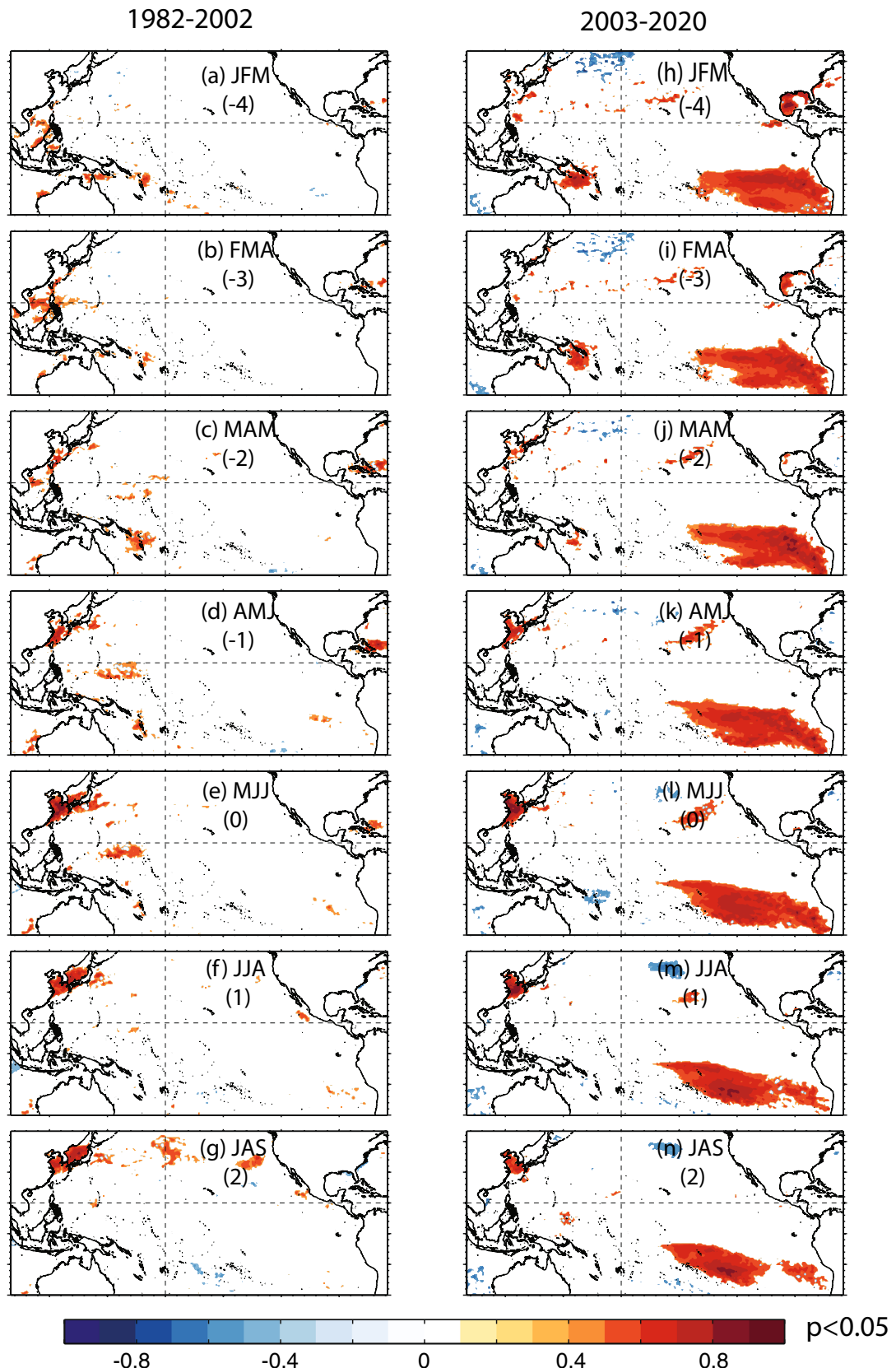
During the period before the regime shift, a region characterized by significant correlations begins to appear during the JFM months in the South China Sea (Fig. 3a), geographically connected upstream of the Taiwan warm current to the YECS through the Taiwan Strait. The region of high correlations seems to move northward to the South China Sea (Fig. 3b–d) and then turns eastward toward the East/Japan Sea and the Northwest Pacific, likely associated with local currents and winds (Fig. 3e–g; Cai et al. 2017; Kim et al. 2018a). In contrast, for the post-regime shift period, a region of robust correlations in the SEP off the coast of Chile emerged almost four months before early summer (Fig. 3h). The correlations reached a maximum of 0.85 at a lag of -2 months (Fig. 3j). Subsequently, the region of robust correlations expands diagonally toward the western Pacific warm pool between the equator and the southern South Pacific Convergence Zone (SPCZ).

3.2 Regressed atmospheric fields onto the summer YECS index

3.2.1 Before the regime shift (1982–2002)

This section investigates atmospheric fields in the context of regime shift. The linear fractions of those variables—SST, precipitation, wind (U850), geopotential height (H850) at 850 hPa, and meridional winds along the date-line—are congruent with the YECS summer SST index (Fig. 4). The magnitudes of the regressed fields represent anomalies corresponding to one standard deviation of the YECS summer SST index. During the pre-2003 period, positively regressed SST anomalies that extend from the YECS toward the center of the North Pacific align with the easterly wind anomalies (Fig. 4a). These wind anomalies represent the weakening of the mean westerly winds over the North Pacific, thus decreasing turbulent heat fluxes into the atmosphere and weakening southward cold Ekman transport, leading to oceanic warming (Yeh and Kim 2010; Cai et al. 2017; Kim et al. 2018a). A positive geopotential height anomaly that locates northeast of the YECS, centered at 42° N and 180° E, and a negative anomaly within the western North Pacific, centered at 140° E and 25° N, seem to generate these easterly wind anomalies in the mid-latitudes. The negative anomaly (i.e., low-pressure anomaly) is accompanied by southwest-northeast-oriented enhanced rainfall throughout the western subtropical North Pacific and suppressed rainfall over the East China Sea and southern East/Japan Sea (Fig. 4b). Another suppressed rainfall anomaly appears in the region west of the dateline around the equator and is associated with a lower-level divergence of the meridional winds and an upper-level convergence around the equator, which is relevant to a descending motion near the equator (Fig. 4b, c).

This low-pressure anomaly in the western North Pacific, accompanied by a tripole structure of precipitation anomalies, bears a resemblance but is opposite to the primary empirical orthogonal function mode estimated from H850 over the Asian-Australian monsoon domain (20° S– 40° N/ 30° E– 180° E; refer to Fig. 2a, b in Wang et al. 2013). This pattern represents the southwest-northeast tilted WNPSH. This spatial analogy implies the role of the eastern equatorial Pacific and northern Indian Ocean in shaping the EASM by modulating the tilted WNPSH during the period before the regime shift (Wang et al. 2000, 2013; Yim et al. 2008; Xiang et al. 2013; Xie et al. 2016). However, the teleconnected influence of the eastern equatorial Pacific and Indian Ocean on the YECS SST anomalies seems statistically insignificant during the early period before the regime shift, as shown in Figs. 2 and 3.



◀Fig. 3 Maps of lagged correlation coefficients between the early summer (MJJ) YECS SST index and lagged SST anomalies for the periods of (a) 1982–2002 and (b) 2003–2020. The correlations above the 90% confidence level are shaded. The numbers in parentheses indicate the number of lagged months

3.2.2 After the regime shift (2003–2020)

This weak coupling is no longer pertinent in summers between 2003 and 2020, after the regime shift (Fig. 4d–f). The high SST regression that previously extended from the YECS to the central North Pacific is confined within the YECS (Fig. 4d). This SST regression in the YECS accompanies with a positive geopotential height anomaly of 4 m and a negative precipitation anomaly higher than -1.6 mm/day . Although the YECS summer SST index is regressed, in recent years, remarkable atmospheric and oceanic signals, such as a zonal dipole pattern of high and low geopotential heights from west to east over the Indian and Pacific Oceans (Fig. 4e), locate in the Southern Hemisphere. This large-scale atmospheric circulation field invokes southerly winds from the south over the SWI and southwestern tropical Pacific, resulting in negative SST anomalies, while northerly wind anomalies from the equator in the southeastern tropical Indian and SEP regions (Fig. 4d) contributing to positive SST anomalies. This large-scale atmospheric circulation resembles the role of air-sea turbulent fluxes in forming a wave-like subtropical dipole in the Southern Hemisphere (Wang 2010). This tropical SST variation, particularly in the SEP, could be enhanced by the WES feedback (Zhang et al. 2014a) and interactive ocean dynamics (Okumura 2013) and contribute to the convective precipitation in the western equatorial Pacific around the dateline (enhanced rainfall) and ITCZ (reduced rainfall) by affecting the meridional winds (Fig. 4e, f; see Sect. 4.1 for a more detailed discussion).

One of the most important features during the recent period is the hemispheric symmetry in both H850 and precipitation over the Pacific Ocean, as shown in Fig. 4e. First, both hemispheres have meridional dipole patterns of positive and negative pressure anomalies from high to low latitudes. The pressure pattern in the Southern Hemisphere is called the South Pacific Oscillation (SPO), with a meridional dipole pattern and barotropic structure throughout the troposphere over mid-to high latitudes (You and Furtado 2017; Fig. 4e, f). In addition, a weak high-pressure anomaly over the YECS corresponds to one occupying the east of Australia. In the precipitation field, the hemispheric symmetry appears to be centered with a negative precipitation anomaly on the ITCZ around 7° N . This is associated with the divergence of low-level winds, as shown in Fig. 4f. Outside the ITCZ, a band of intensified rainfall appears as a tilted feature in the north of the SPCZ, with a weaker band extending toward the center of the North Pacific. On the poleward side,

negative anomalies are located over the SPCZ in the Southern Hemisphere and a northeastward-tilted region from the East China Sea in the Northern Hemisphere.

The characteristic structures shown in Fig. 4d, e, i.e., off-equatorial weakened southeasterly trade winds and a meridional SST dipole pattern in the SEP accompanied by the SPO and the hemispheric symmetrical pattern, exactly match the atmospheric-oceanic signatures of the SPMM (Zhang et al. 2014a; Min et al. 2017; Larson et al. 2018; Amaya 2019; see Fig. 1b of Zhang et al. 2014a), known as the EP El Niño precursor (Zhang et al. 2014a; Min et al. 2017; You and Furtado 2017) or a modulator of the ENSO amplitude (Imada et al. 2016; Larson et al. 2018). The EP El Niño signature normally overwhelms this meridional mode; therefore, the SPMM is analogous to a typical El Niño-like pattern in the presence of ocean-involved dynamics within the equatorial Pacific (Zhang et al. 2014a; Min et al. 2017; You and Furtado 2017).

3.2.3 Regressed atmospheric fields onto the SPMM index

Figure 5 shows the same regressed fields as in Fig. 4, but for onto the standardized MJJ averaged SST anomaly over the SEP region. We defined this time series as the SPMM index. After the regime shift, the general patterns of the regressed fields are almost identical to those regressed onto the YECS SST index (compare Fig. 5d–f with Fig. 4d–f). On the other hand, before the regime shift, the SPMM exhibits an El Niño-like pattern as expected from previous studies: the convergence of regressed winds east of 150° E is accompanied by reinforced precipitation and warm SST anomalies over the central to eastern equatorial Pacific (Fig. 5a–c). Concurrently, a subtropical high-pressure system juxtaposed with robust depressed precipitation appears in the western North Pacific. This spatial structure also shows a typical southwest-northeast tilted WNPSH pattern, whose northern rim delimits the southern boundary of the YECS around 30° N , implying a limited influence of the equatorial signature on the YECS SST anomalies.

The periods before and after the regime shift are short, less than 20 years, possibly resulting in uncertainties in our argument because of internal atmospheric noise and external climate feedback processes. We assessed the robustness of our results by taking advantage of SST-forced numerical experiments based on the Norwegian Climate Prediction Model version 1 (NorCPM1; Bethke et al. 2021). This model has ten ensemble members over the longest period spanning up to 2018 among the Atmosphere Model Intercomparison Project (AMIP) phase 6 simulations. Although the observed (Fig. 5) and simulated (Fig. S4) fields that were regressed onto the summer SPMM index show a slight discrepancy in spatial distribution and magnitude, the overall similarities in the regressed

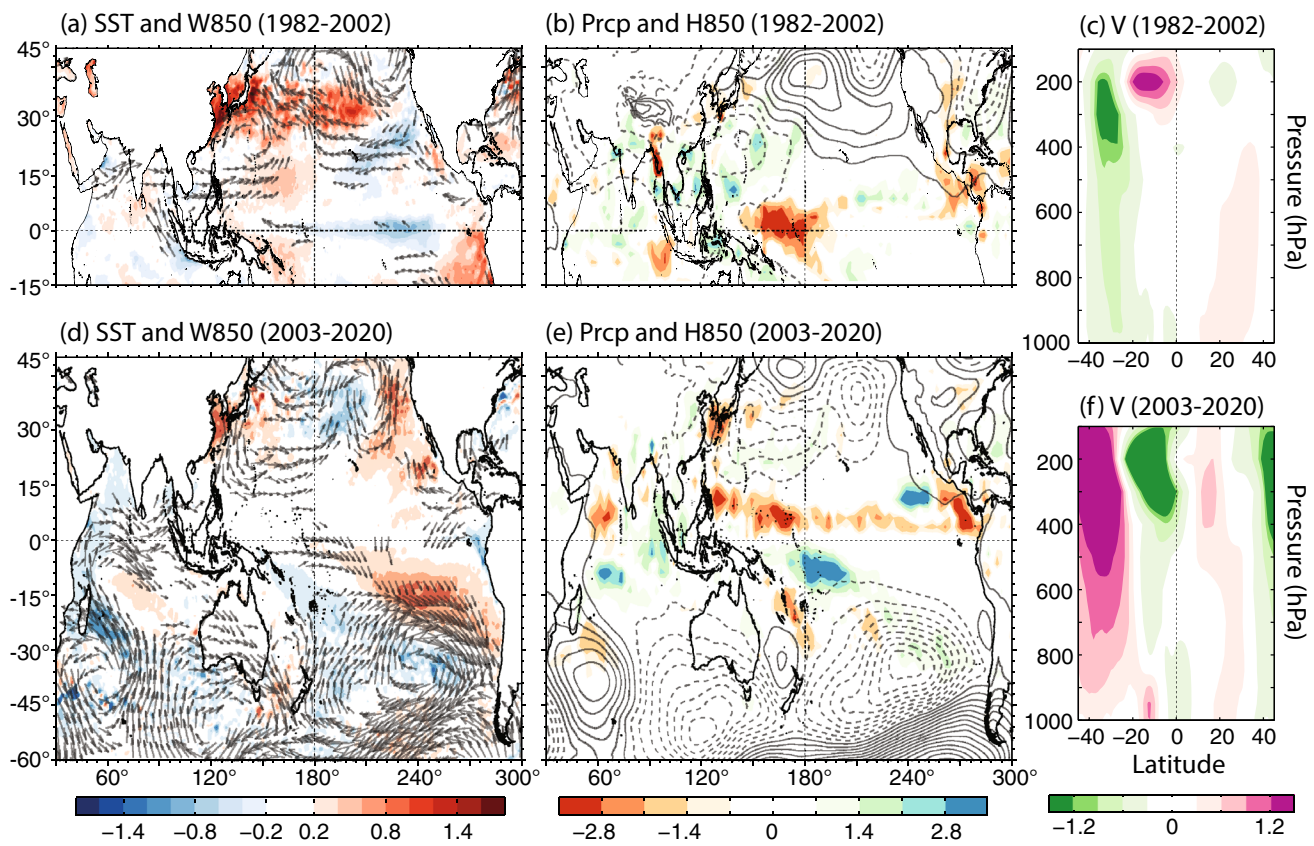


Fig. 4 Regressed anomalies of **a** SST (color, unit: $^{\circ}\text{C}$), wind (vector, m/s), **b** geopotential height (contour, m) at 850 hPa, precipitation (shading, mm per day), and **c** meridional wind (m/s) at the dateline on the YECS summer SST index for the period 1982–2002. **d–f** represent the same anomalies as **a–c** but for the period 2003–2020. The contour interval for the geopotential height anomalies at 850 hPa is 4 m, the negative contours are dashed, and the zero contour is omitted

represent the same anomalies as **a–c** but for the period 2003–2020. The contour interval for the geopotential height anomalies at 850 hPa is 4 m, the negative contours are dashed, and the zero contour is omitted

rainfall also highlight the role of the SST anomaly in the SEP region in generating the interhemispheric SEP–YECS coupling.

Owing to the similarity between the SPMM and ENSO, studies on this meridional mode have devoted substantial efforts to removing ENSO signals, for instance, by adopting linear regression to separate the cold tongue index from the reanalysis dataset (Chiang and Vimont 2004; Min et al. 2017); by coupling a slab ocean mixed layer model to remove oceanic dynamics, thus pulling apart the Bjerknes feedback and Rossby wave adjustments (Zhang et al. 2014a); and by prescribing climatological winds with no anomalous ENSO-related forcing to the ocean model (Larson et al. 2018; Zhang et al. 2021). Because we did not attempt to remove oceanic dynamics, the ENSO-like signature before the regime shift was consistent with previous studies. Unexpected is the independent SPMM pattern after the regime shift. As argued in several previous studies, the emergence of the SPMM signature in recent years suggests that the amplitude of the canonical ENSO has been substantially reduced after the early 2000s (McPhaden 2012; Kohyama

et al. 2017; Li et al. 2019). This hypothesis is investigated further in the following section.

3.3 SPMM-related modes before and after the regime shift

An SVD analysis was applied to a cross-covariance matrix between the MJJ SST in the tropical Pacific domain (20°S – 20°N / 140°E – 70°W) and the MJJ precipitation in the western Pacific (20°S – 50°N / 110°E – 150°W) to investigate systematic changes in the equatorial Pacific and western North Pacific. Figure 6 illustrates the SPMM-related SVD modes and their corresponding principal components: the primary mode before the regime shift and the third mode after the regime shift. These selections were based on that the SPMM index covaried with the PC1 before the regime shift ($r = -0.61$) and PC3 after the regime shift ($r = 0.78$) (see Fig. 6b, e). These correlations are significant at the 95% confidence level.

The SST spatial pattern of the primary mode before the regime shift shows a cold tongue pattern that extends from

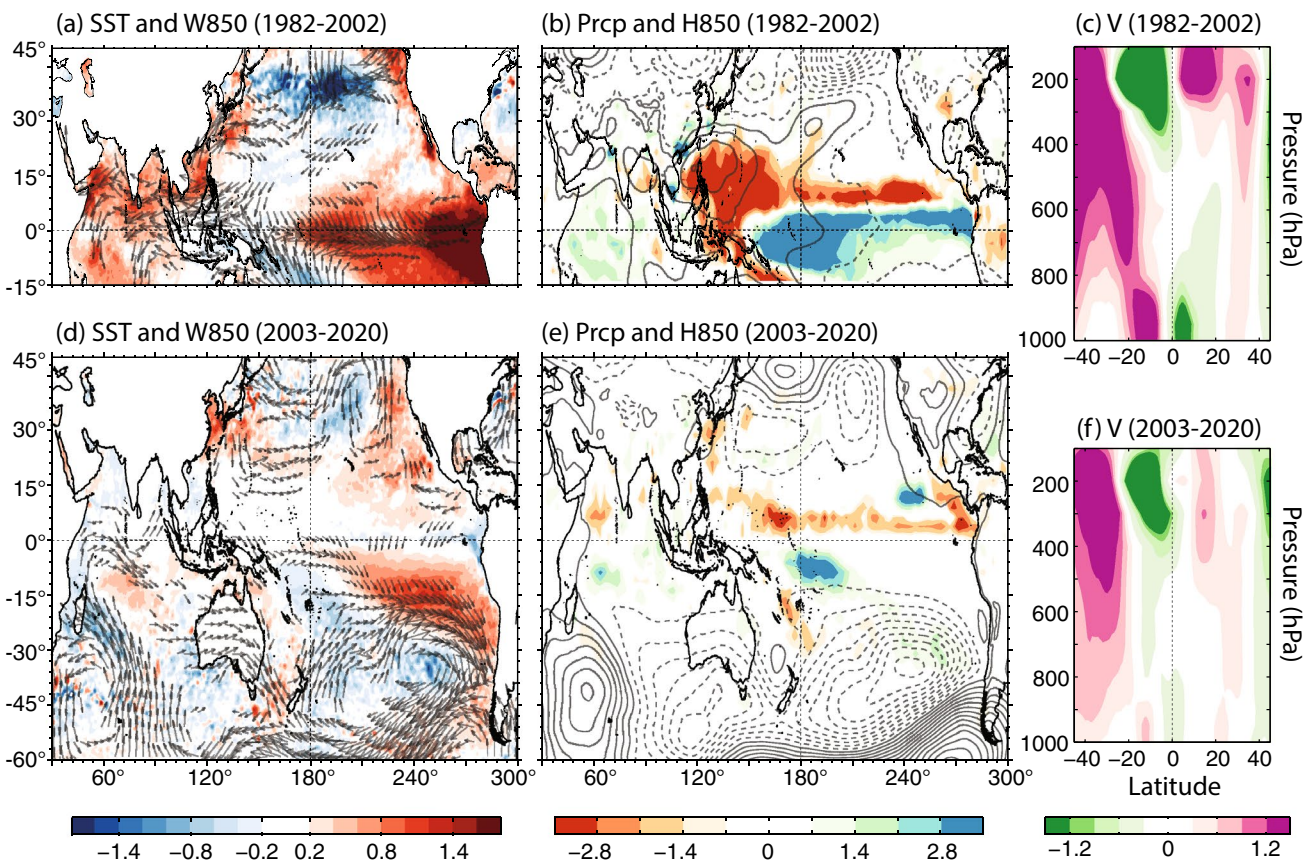


Fig. 5 Represents the same data as Fig. 4, but it shows regression onto the MJJ mean Southeastern Pacific SST anomalies

the equatorial eastern Pacific, indicating that this mode is also relevant to the EP El Niño (i.e., the correlation coefficient between the SST PC1 and Nino3 index is -0.98). The corresponding rainfall pattern is also a typical southwest-northeast tilted pattern of the WNPSH. The correlation coefficient between the principal components of SST and precipitation is 0.92, suggesting a robust coupling between the EP El Niño-like pattern and precipitation over the western North Pacific. The analogy between Figs. 5b and 6a demonstrates that the EP El Niño-related WNPSH partially determined the EASM before the regime shift, in agreement with previous findings such as those by Yim et al. (2008) and Wang et al. (2013). This primary EP El Niño-WNPSH coupling mode explains approximately half (48.5%) of the square covariance between the two fields.

The primary SVD mode for the 2003–2020 period is also an El Niño-like pattern but with extra loading in the central equatorial Pacific; its corresponding rainfall pattern changes with increased precipitation over the western Pacific warm pool instead of over the WNPSH region (see Fig. S5). Notably, there is a substantial decrease in the square covariance in SVD1, which accounts for only 31.0% of the square covariance during the recent period, which is

an approximately 20% decrease in the explained percentage by this mode during the period before the regime shift. The SPMM-related pattern appears in the third mode after the regime shift (Fig. 6d–f). Although the contribution of this mode to the total variability is 14.3%, a robust correlation higher than 0.80 between the PCs of SST and precipitation demonstrates a robust coupling between the SST over the SEP and the rainfall in the western North Pacific. Intriguingly, the rainfall pattern of SVD3 (Fig. 6d) shows a meridional dipole pattern over the western tropical Pacific, along with depressed precipitation over the YECS. This horizontal pattern is analogous to the regressed rainfall patterns on the YECS SST index (Fig. 4e) and SPMM index (Fig. 5e).

Our results indicate that the ocean and atmospheric signals appearing in the western North Pacific is large-scale atmospheric responses to tropical precipitation changes (Deser and Phillips 2006; He et al. 2011; Wu et al. 2015; Liu et al. 2018). The SVD analysis, regressed fields as shown in Fig. 5, and previous articles collectively demonstrate that the SPMM, which is independent of but somewhat resembles and interacts with ENSO (Zhang et al. 2014a), had an ENSO-like signature between 1982 and 2002. This situation changed in the early 2000s. The SPMM emerges as a

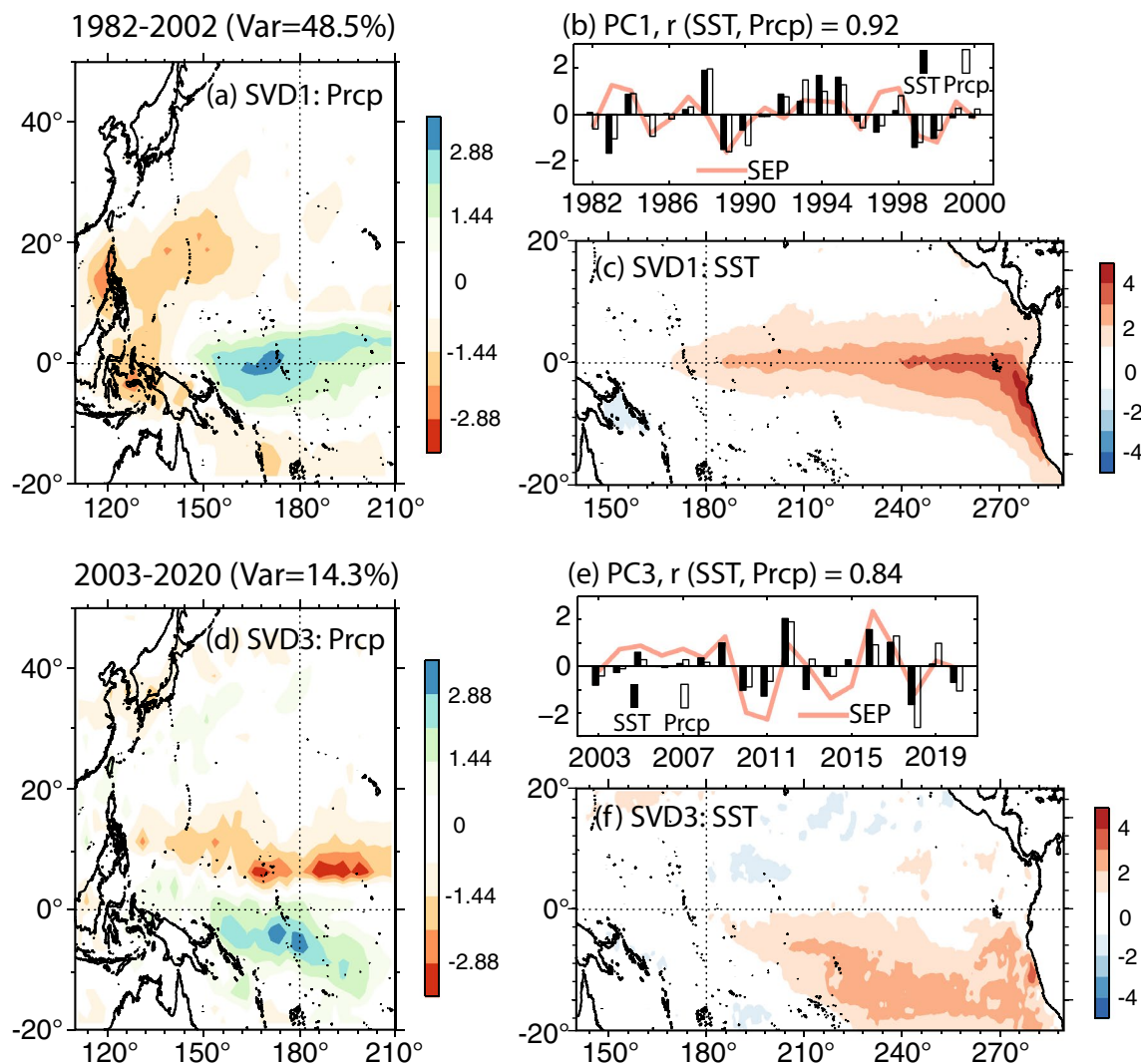


Fig. 6 Spatial structures of SVD1 between the MJJ mean precipitation anomalies over the region 20°S–50°N/110°E–150°W and the tropical Pacific SST anomalies over the region 20°S–20°N/140°E–70°W for **a** precipitation (mm per day), **c** SST (°C), and **b** their

corresponding principal components during the period 1982–2002. **d–f** represent the same anomalies as **a–c**, respectively, but for 2003–2020. The red lines in **b** and **e** are the MJJ mean SST anomalies over the southeastern Pacific (SEP: 20°S–10°N/130°W–100°W)

visible mode because the dominant El Niño signatures have been substantially weakened. It means that the mean state of the equatorial Pacific is a La Niña-like condition (Kohyama et al. 2017).

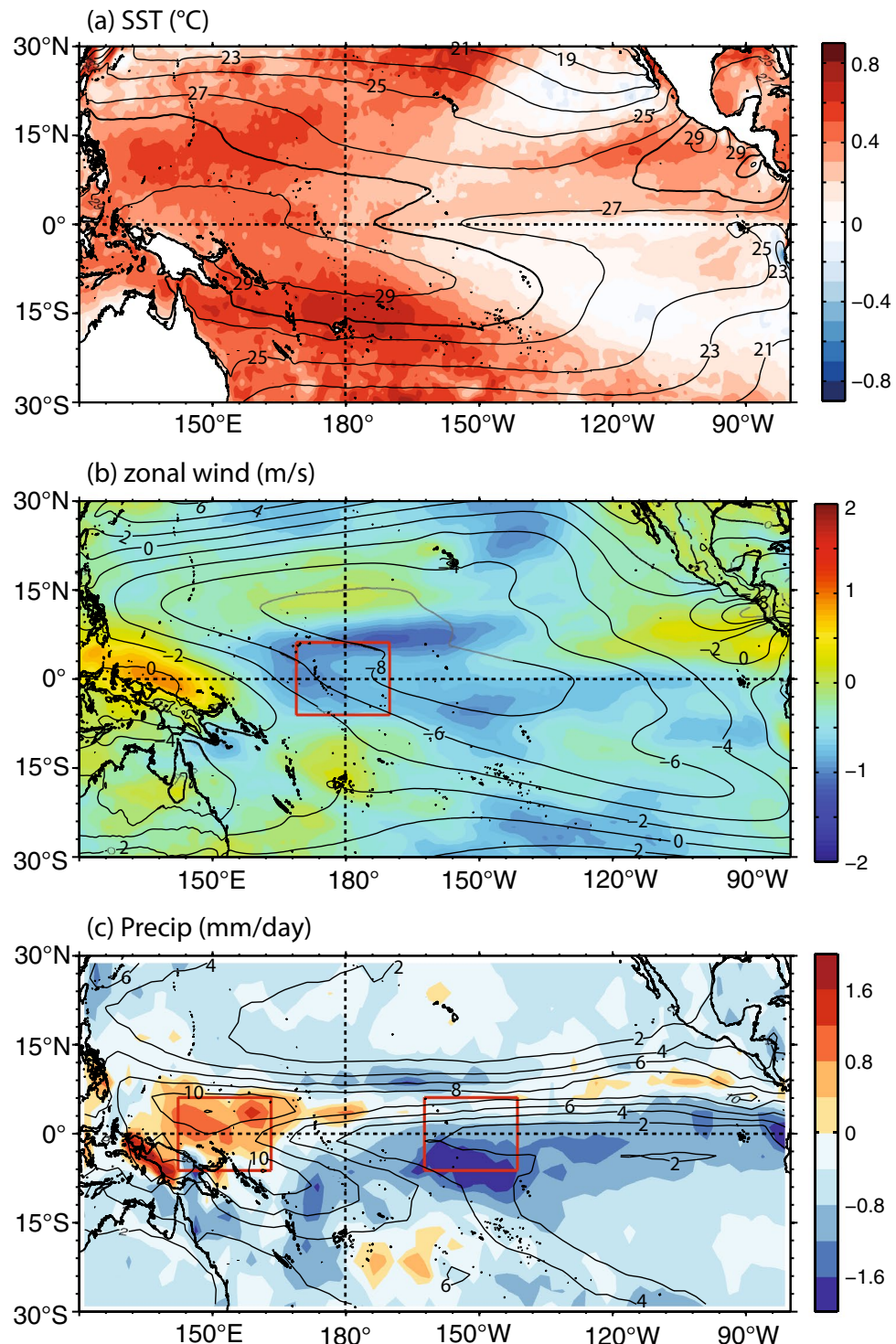
4 Discussion

4.1 Atmospheric bridge for the interhemispheric connection during the La Niña-like mean state

To elucidate the systematic change in the tropical Pacific during the early 2000s, we estimated the epoch differences between the two periods, that is, the recent period of 2003–2020 minus the early period of 1982–2002, for

SST, zonal winds at the 850 hPa level, and precipitation (Fig. 7). As the summer SST of the Y ECS is relevant to the SEP anomalies for extended months, as depicted in Fig. 3, we illustrate the mean differences averaged from February to July. These spatial patterns of epoch differences are not sensitive to month selection. The SST difference shows that the western tropical Pacific warms more than the eastern tropical Pacific, with the highest warming of up to 0.8 °C in the southwestern tropical Pacific around the dateline. Weak but cold anomalies emerge over the cold tongue region and the SEP off the coast of Chile and over the northeast subtropical Pacific off the California coast, toward the central equatorial Pacific. This SST difference pattern coincides with trade winds that strengthen by 12.5% relative to that in the period before the regime

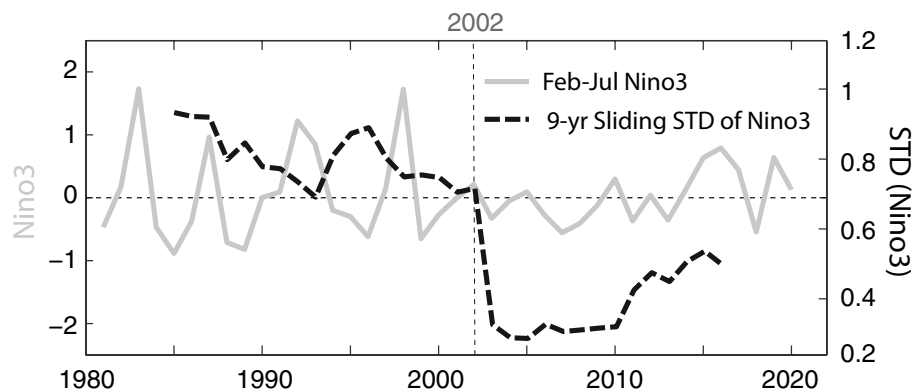
Fig. 7 Epoch difference map of the February–July mean **a** SST from OISSTv2, **b** zonal wind at 850 hPa from ERA5, and **c** precipitation from CMAP, obtained by subtracting those for 1982–2002 from those for 2003–2020. The epochal differences in the zonal wind and zonal precipitation gradient are estimated over the regions in the red boxes in **b** and **c**, respectively



shift (the red box in Fig. 7b); the zonal precipitation gradient around the central equatorial Pacific was enhanced by 22.3% (Fig. 7c). These results collectively reflect that the Walker circulation was intensified for the post-2003 period relative to the previous period, suggesting a La Niña-like mean state during the period after the regime shift. The strength of El Niño events tends to fluctuate substantially

hence rendering large variance for the El Niño-like mean state whereas that of La Niña events remains steady hence low variance for the La Niña-like mean state (Kohyama et al. 2017). This nonlinear characteristic of ENSO activity (An and Jin 2004) is examined by applying a sliding standard deviation to the February to July mean Nino3 SST index (Fig. 8). The standard deviation of the Nino3 index

Fig. 8 February to July mean Nino3 time series (solid gray line) and its 9-year running standard deviation (dashed black line)



for the early years was greater than 0.7, then decreased drastically to approximately 0.3 across the early 2000s, indicating that the background tropical Pacific state shifted suddenly from an El Niño-like to La Niña-like regime. This decadal shift is consistent with evidence from previous studies that have demonstrated an overall weakening of thermodynamic variability in the eastern equatorial Pacific in recent years (Hu et al. 2017). This includes the decreased transport of oceanic heat from the western warm pool region to the eastern equatorial Pacific via suppressed oceanic Kelvin waves, in association with a weakening of the low-level westerly winds (or a westward shift of the atmosphere–ocean coupling) in the central and eastern tropical Pacific (Li et al. 2019), reduced oceanic thermocline feedback (Guan and McPhaden 2016), and intensified thermal stratification within the upper ocean in the eastern equatorial Pacific (Imada et al. 2016; Hu et al. 2017; Kohyama et al. 2017).

An important question that needs to be answered is how the air-sea signals in the SEP have crossed the equator and reached the extratropics of the Northern Hemisphere. Previous studies have argued that interhemispheric teleconnection might be determined by modulating the large-scale atmospheric circulation around the ITCZ (Trenberth et al. 1998; Deser and Phillips 2006; Zhang et al. 2014b; Wu et al. 2015; Liu et al. 2018). The fact that the ITCZ is located north of the equator at approximately 7° N for most of the year allows the propagation of the SST signals over the SEP toward the central to western tropical Pacific through the WES and wind-driven meridional circulation (Gu and Philander 1997; Toniazzo 2010; Okumura 2013; Zhang et al. 2014a). The positive SST anomalies in the western tropical Pacific warm the air above, raise the surface air into the atmosphere, and lead to convective precipitation (Sarthi and Kumar 2022). This process represents a change in the convective forcing in the tropics that affects large-scale (or stratiform) rainfall over East Asia by redistributing the vertical structures of atmospheric temperature, momentum, moisture, and horizontal moisture transport (Gao and Li 2008; Yang et al. 2021).

Figure 9 shows the lagged regression of anomalous precipitation components for convective (left column) and large-scale (right column) precipitation onto winter (i.e., JFM months) mean SST anomalies in the SEP region. These two types of precipitation, estimated by the convection and cloud schemes of the ECMWF model, constitute total precipitation (Hersbach et al. 2020). The selection of the JFM months was based on the significant relationship between the MJJ mean YECS SST anomalies and the YECS SST anomalies for these months, shown in Fig. 3. As illustrated by the SVD analysis above, increased precipitation throughout the region between the ITCZ and SPCZ, along with the accompanying compensated, suppressed precipitation over the convergence zones, is remarkable in the regressed fields for the convective component (left column of Fig. 9). The maximum convective precipitation anomalies appear for a one- or two-month lagged field (Fig. 9b, c) and seem to last until the summer months (Fig. 9e), demonstrating that the convective precipitation changes in the western tropical Pacific follows SST variance over the SEP by one or two months. As an extratropic response to convective precipitation over the tropical Pacific, the large-scale precipitation component appears to decrease over the western North Pacific and finally over the YECS during the spring and summer months (Fig. 9j–l).

The precipitation index is quantitatively portrayed as the difference in the standardized winter (JFM) average convective precipitation between the two boxes, as shown in Fig. 9a (red minus blue boxes). Figure 10 illustrates the regression fields of the low-level (i.e., 1000 hPa) divergence anomaly of the winds with a superposed 850 hPa geopotential height anomaly on the winter SPMM index (the SST anomaly averaged over the SEP; left-hand column in Fig. 10) and on the precipitation index (right-hand column). Immediately apparent is that the large-scale atmospheric responses to the winter SPMM index in the Northern Hemisphere (Fig. 10a) are analogous to those for convective precipitation in the tropical Pacific (Fig. 10g), with negative geopotential height signals at high latitudes in both hemispheres and a positive

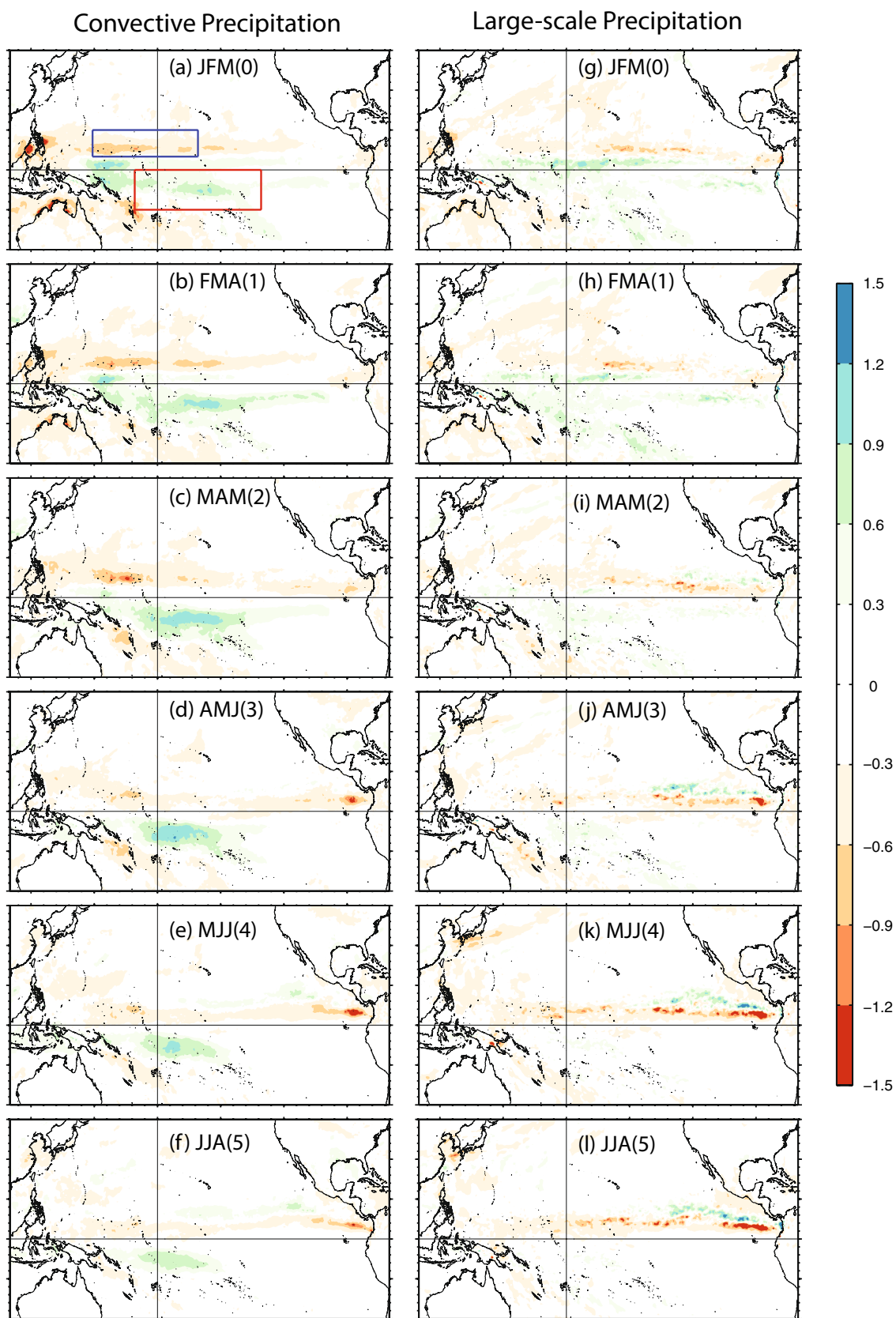
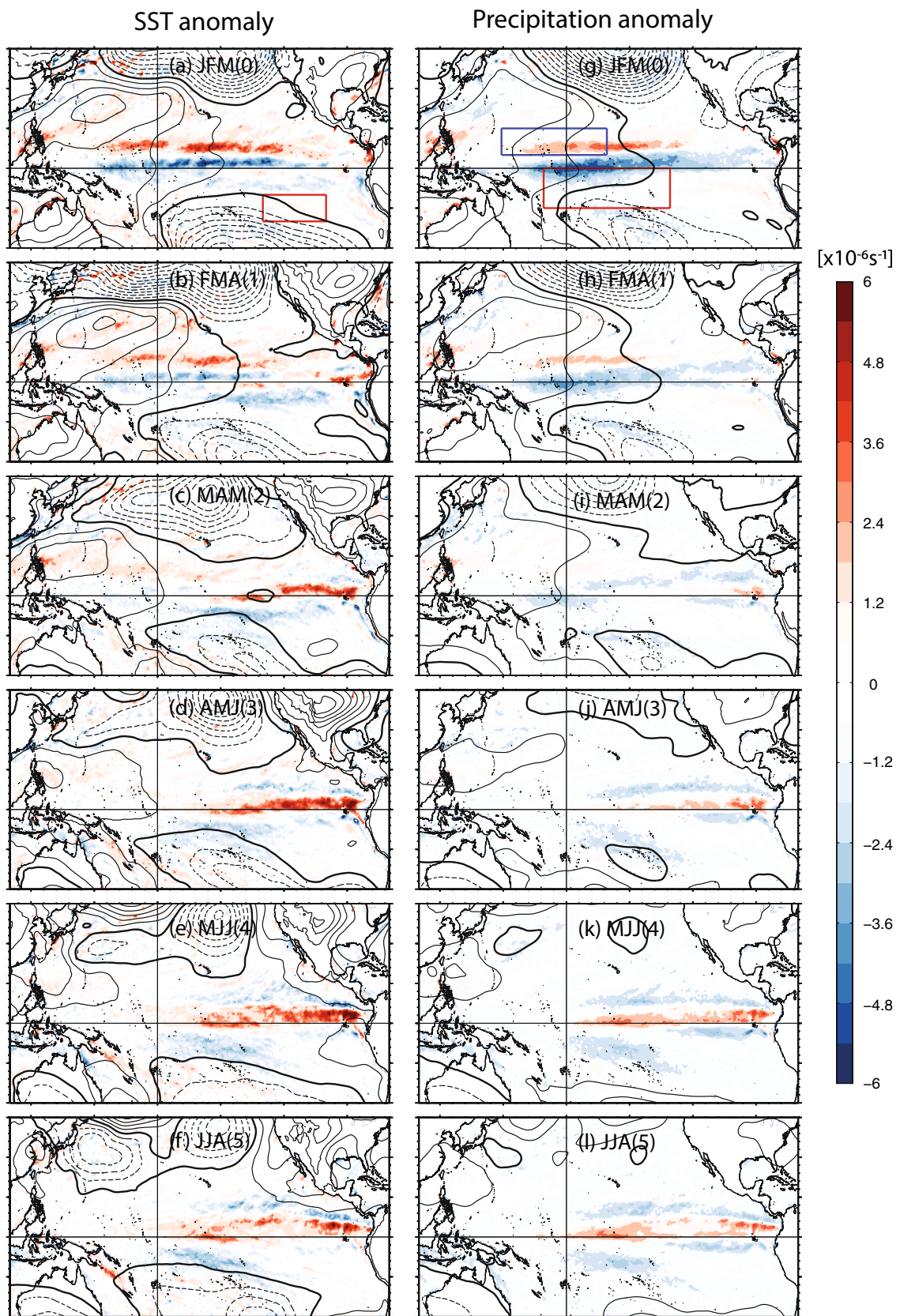


Fig. 9 Lagged linear regression of the (a–f) convective (g–l) large-scale components of the precipitation (unit: mm per day) on the JFM mean SST anomalies over the SEP region for the post-2003 period. The boxes in a indicate the domains for the precipitation index in Fig. 10



◀Fig. 10 Lagged linear regression of the divergence of 1000 hPa winds (shading: s^{-1}) and geopotential height anomalies at 850 hPa (contour) on the JFM mean (a–f) SEP index and (g–l) precipitation index for the post-2003 period. The SEP index is estimated for the mean SST over the red box domain in a, and the precipitation index for the mean convective precipitation difference between the red and the blue boxes in g. The contour interval for the geopotential height anomalies is 6 m, the negative contours are dashed, and the zero contour is indicated by the thick line

one over the western North Pacific. This result demonstrates that the precipitation anomaly in the western tropical Pacific could act as an atmospheric bridge between the SEP and northwestern Pacific. Upon close inspection, it appears that the response to the SPMM in the Northern Hemisphere has a maximum for a one-month lagged field (Fig. 10b) whereas that for the western tropical convective precipitation has no such lag. Our interpretation is that the air-sea interactive signals over the SEP region reach the equator in a period of one month and then spontaneously modulate large-scale atmospheric circulation in the extratropical North Pacific by altering western tropical precipitation. Another remarkable feature in Fig. 10 is the anticyclonic circulation anomaly over the western North Pacific, that is, the WNPSH, during the JFM to AMJ seasons (Fig. 10a–d). Wang et al. (2000) illustrate that the warming anomaly over the central equatorial Pacific can initiate the WNPSH, which could be maintained by air-sea interactions in the western North Pacific. This WNPSH forms anomalous southwesterly winds, resulting in a positive SST anomaly over the YECS by bringing in warm air from the south. Figure 11 shows a schematic diagram illustrating how the off-equatorial wind-induced SST signal over the SEP reaches the YECS through modulating the western tropical precipitation fields and the WNPSH.

4.2 Susceptibility of the YECS to atmospheric forcing

Why does the SST footprint of the SPMM emerge in the YECS? This emergence is unexpected, particularly when considering that the most remarkable pressure anomaly for the SPMM appears in the central North Pacific around the Aleutian Islands (Figs. 4e, 5e, and 10). The SPMM footprint within the YECS indicates its susceptibility to stochastic atmospheric forcing, as noted by Zhang et al. (2010). The shallow water depth of the YECS (i.e., an average depth of only 75 m) partially accounts for this susceptibility (Yeh and Kim 2010; Kim et al. 2018a) in contrast to deep oceans, in which intrinsic variability is more critical than atmospheric stochastic forcing owing to its large thermal inertia.

Another reason might be the positive feedback process between solar radiation, stratification, and turbulent tidal mixing in the YECS (Kim et al. 2022). An initial warm perturbation at the sea surface creates a buoyant surface layer

within which solar radiation is effectively trapped, intensifying the vertical stratification of the layer. Enhanced stratification restricts the tide-induced stirring effect within the bottom layer, which normally dissipates an anomalous surface signal into the bottom layer through turbulent tidal mixing and entrainment. The reduced exchange across the thermocline enhances surface warming and bottom cooling, further enhancing stratification. This positive feedback seems to enlarge and prolong surface temperature anomalies, often causing marine heatwave events observed during recent summers over the YECS (Gao et al. 2020). In contrast, an initial cold surface perturbation weakens the stratification and promotes vertical exchange through turbulent tidal mixing and entrainment, resulting in enhanced surface cooling and bottom warming anomalies. This vertical temperature modulation further reduces the stratification, which also constitutes positive feedback.

Intense summer rainfall associated with the Changma-Meyu rain band that tends to occur over four to six weeks in June and July (Ha et al. 2012) could fortify this positive feedback. Owing to intense rainfall, substantial riverine runoff tends to create a buoyant plume that spreads throughout the YECS (Belkin 2009; Lie et al. 2003). This plume tends to generate a barrier layer between the thermocline and the surface-mixed layer (Kim et al. 2018b, 2019). This layer more effectively restrains the exchange of momentum and heat, intensifying the positive feedback (Belkin 2009; Park et al. 2011). For example, the air-sea monitoring system at the Ieodo Ocean Research Station, situated at the center of the East China Sea (Ha et al. 2019), detected an abrupt increase in surface temperature from 26.5 to 28.0 °C on August 06, 2021, as riverine waters, at least 5 psu fresher than the ambient waters, reached the station. The water temperature then increased steadily to 31 °C in three weeks owing to the positive feedback. Typhoon Bavi, which passed the YECS on August 26, terminated this marine heatwave by causing intense vertical mixing and reducing the surface temperature by 7 °C.

5 Summary and concluding remarks

This study was motivated to explain why the reported ENSO-induced YECS SST modulation was weak and the forcing region was inconsistent in the literature. We have explored this question by assuming a decadal change in the tropical Pacific's mean state around the early 2000s and the existence of ENSO's precursor (i.e., the meridional modes). Consistent with these hypotheses, we found a regime shift in the decadal relationship between the summer (MJ) mean SST in the YECS and tropical Pacific anomalies.

A canonical EP El Niño-like signature was prevalent and overwhelmed the air-sea interacted variability in the

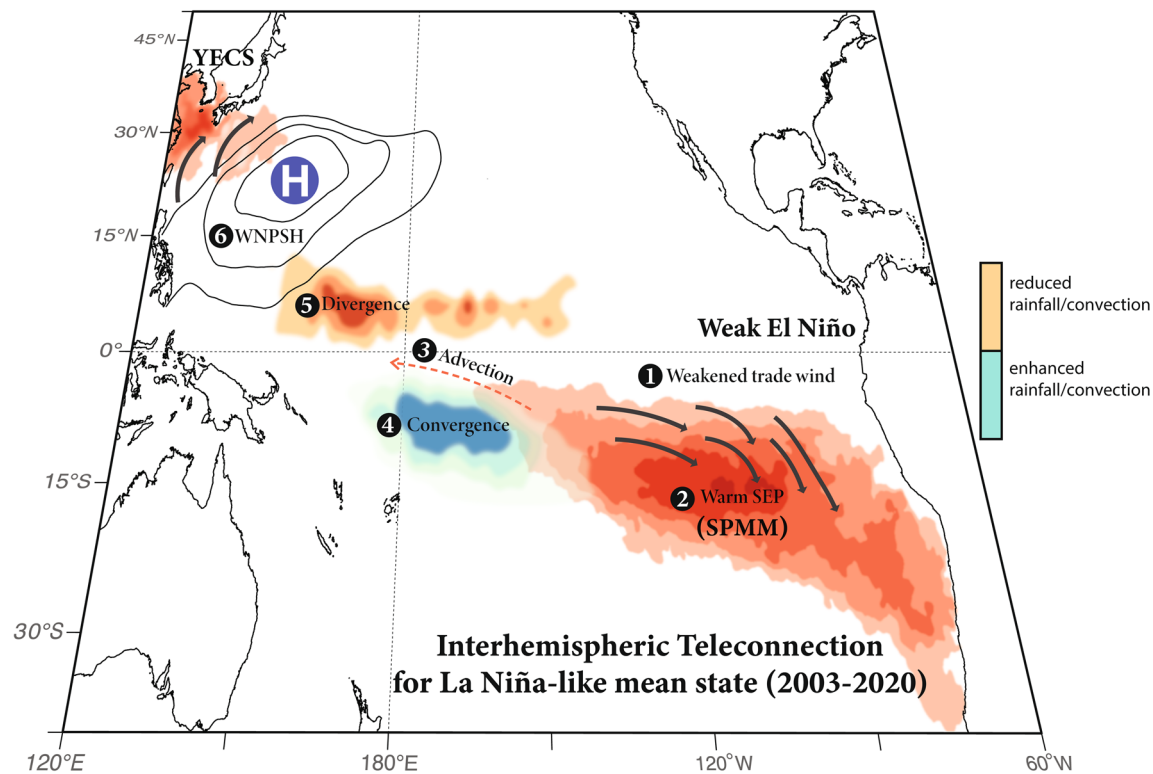


Fig. 11 Schematic diagram for interhemispheric teleconnection between the Southeastern tropical Pacific (SEP) and the Yellow and East China Seas (YECS) during the La Niña-like mean state of 2003–2020. During this period, ① weakened trade winds cause a ② warm sea surface anomaly within the SEP. ③ Through the wind-evaporation-SST feedback and background currents, the warm anomaly propagates into the central equatorial Pacific, which in turn results

in ④ enhanced convection and increased rainfall between the ITCZ and SPCZ. This anomalous convection acts to ⑤ suppress convective activity in the western tropical Pacific along the ITCZ. The resulting divergence flow triggers the ⑥ WNPSH, and the warm air advection associated with anomalous WNPSH leads to a positive SST anomaly over the YECS

SEP–SPMM before the early 2000s. The ENSO-related WNPSH (Wang et al. 2013) partially regulated the meridional winds and precipitation over the EASM region. This ENSO-related atmospheric modulation in the western North Pacific, however, had an insignificant effect on SST in the YECS. In contrast, during the post-2003 era, when the mean state of the equatorial Pacific reverted to La Niña-like conditions, the SPMM, initiated by an off-equatorial wind-induced SST anomaly associated with an anomalous South Pacific subtropical high, emerges as a visible mode separated from the ENSO. We believe that convective precipitation over the western tropical Pacific acts as an atmospheric bridge to mediate this interhemispheric teleconnection and to induce an upward motion in the troposphere, resulting in increased convective precipitation between the ITCZ and SPCZ regions and suppressed rainfall over these convergence zones. This convective forcing renders a subsequent atmospheric response in the extratropical regions in both hemispheres (Trenberth et al. 1998; Deser et al. 2004; Deser and Phillips 2006), causing hemispheric symmetric patterns in geopotential height and precipitation fields (Zhang et al.

2014a). The SPMM-induced WNPSH anomaly yields southwesterlies of warm air from the south, resulting in a positive SST anomaly over the YECS.

The present study focuses on the interannual variance of the SPMM owing to the lack of reliable multidecadal SST time series. However, previous studies have underlined the critical role of stochastic forcing from weather systems in the Southern Hemisphere (Okumura 2013; Liguori and Di Lorenzo 2019; Zhang et al. 2021) in driving decadal ENSO-like variability. The long-term modulation of the ENSO-mean state reminds us of a positive-to-negative phase shift of the Interdecadal Pacific Oscillation (IPO), the leading mode of tropical Pacific decadal variability (Okumura et al. 2017), around the year 2000 (Dong and Dai 2015; Hu et al. 2017; Dong et al. 2018; Li et al. 2019). Meanwhile, AMO-related warming in the tropical Atlantic could also induce cooling in the eastern Pacific, thus strengthening the Pacific Walker circulation (Ham et al. 2013; England et al. 2014; McGregor et al. 2014). The phase-synchronized shift of the Hadley and Walker circulations amplifies the AMO-induced Pacific Walker circulation (Yun et al. 2021), presumably leading to

the La Niña-like mean state. Kohyama and Hartmann (2017) proposed a nonlinear ENSO warming suppression (NEWS) mechanism to show that La Niña-like mean state warming is also a likelihood candidate for warm climates because of the nonlinear rectification effect (An and Jin 2004). If the NEWS mechanism is pertinent to future projections, SPMM–YECS coupling may become more common with global warming (Ashok et al. 2012; Imada et al. 2016). However, future projections are controversial in climate models (Kohyama et al. 2017; Yang et al. 2021; Cai et al. 2021). Therefore, the following issues require attention: the future tendencies of the SPMM under global warming; the decadal variation of the SPMM and its impact on climates, such as the ENSO type and the hiatus of global warming; the decadal evolution of the SPMM–YECS coupling; and the cause-effect relationship between the mean state in the tropical Pacific and the frequency of extreme El Niño events.

Supplementary Information The online version contains supplementary material available at <https://doi.org/10.1007/s00382-022-06529-1>.

Acknowledgements The authors wish to thank Dr. Go-Un Kim for helpful discussions and Yongchim Min and Jae-Ik Lee for the temperature and salinity time series observations from the Ieodo Ocean Research Station. We also thank Yoo Dam Son for illustrating the schematic diagram to highlight our key results. The revision of the manuscript benefited from the constructive comments and suggestions made by two anonymous reviewers.

Author contributions YSK, MK, and CJJ designed the study. E-SC conducted and analyzed the simulated results for AMIP6 and CMIP6. J-YJ and YSK processed the time-series data at Ieodo Ocean Research Station. YSK, MK, S-WY, and E-SC interpreted results. YSK and E-SC wrote the manuscript. S-WY and E-SC helped to improve the manuscript.

Funding This work was supported by Korea Institute of Marine Science & Technology Promotion (KIMST) projects entitled “Establishment of the ocean research station in the jurisdiction zone and convergence research (20210607)” and “Study on air-sea interaction and process of a rapidly intensifying typhoon in the northwestern Pacific (2022056)” funded by the Ministry of Oceans and Fisheries, Korea. YSK and CJJ were supported by a National Research Foundation of Korea grant, funded by the Korean Government (NRF-2020R1F1A1070398 and NRF-2020R1F1A1072447). E-SC received support for the project titled “Investigation and Prediction System Development of Marine Heatwave around the Korean Peninsula originated from the Sub-Arctic and Western Pacific,” under the Ministry of Oceans and Fisheries, Korea (PM22090).

Data availability The data used in this work can be downloaded from developers’ or authorized websites.

Declarations

Conflict of interests Authors declare they have no financial interests.

References

- Amaya DJ (2019) The Pacific meridional mode and ENSO: a review. *Curr Clim Change Rep.* <https://doi.org/10.1007/s40641-019-00142-x>
- An S-I, Jin F-F (2004) Why El Niño is stronger than La Niña. *J Clim* 17(12):2399–2412
- Ashok T, Sabin TP, Swapna P, Murtugudde RG (2012) Is a global warming signature emerging in the tropical Pacific? *Geophys Res Lett* 39:L02701
- Bao B, Ren G (2014) Climatological characteristics and long-term change of SST over the marginal seas of China. *Cont Shelf Res* 77:96–106
- Beardsley R, Limeburner R, Yu H, Cannon G (1985) Discharge of the Changjiang (Yangtze River) into the East China Sea. *Cont Shelf Res* 4:57–76
- Belkin IM (2009) Rapid warming of large marine ecosystems. *Prog Oceanogr* 81:207–213
- Bethke I, Wang Y, Counillon F, Keenlyside N, Kimmritz M, Fransner F, Samuels A, Langehaug H, Svendsen L, Chiu PG, Passos L et al (2021) NorCPM1 and its contribution to CMIP6 DCPP. *Geosci Model Dev* 14(11):7073–7116. <https://doi.org/10.5194/gmd-14-7073-2021>
- Bond NA, Overland JE, Spillane M, Stabeno P (2003) Recent shifts in the state of the North Pacific. *Geophys Res Lett* 30(23):2183. <https://doi.org/10.1029/2003GL018597>
- Bretherton CS, Widmann M, Dymnikov VP, Wallace JM, Bladé I (1999) The effective number of spatial degrees of freedom of a time-varying field. *J Clim* 12(7):1990–2009
- Cai R, Tan H, Kontoyiannis H (2017) Robust surface warming in offshore China Seas and its relationship to the East Asian Monsoon wind field and ocean forcing on interdecadal time scales. *J Clim* 30:8987–9005. <https://doi.org/10.1175/JCLI-D-16-0016>
- Cai W, Santoso A, Collins M et al (2021) Changing El Niño-Southern Oscillation in a warming climate. *Nat Rev Earth Environ* 2:628–644. <https://doi.org/10.1038/s43017-021-00199-z>
- Capotondi A, Wittenberg AT, Newman M, Di Lorenzo E, Yu JY, Braconnot P et al (2015) Understanding ENSO diversity. *Bull Am Meteorol Soc* 96:921–938. <https://doi.org/10.1175/BAMS-D-13-00117.1>
- Chang P, Zhang L, Saravanan R, Vimont DJ, Chiang JCH, Ji L, Seidel H, Tippett MK (2007) Pacific meridional mode and El Niño-Southern Oscillation. *Geophys Res Lett* 34:L16608. <https://doi.org/10.1029/2007GL030302>
- Chiang JCH, Vimont DJ (2004) Analogous Pacific and Atlantic meridional modes of tropical atmosphere-ocean variability. *J Clim* 17:4143–4158. <https://doi.org/10.1175/JCLI4953.1>
- Choi Y, Ha K-J (2018) Subseasonal shift in tropical cyclone genesis over the western North Pacific in 2013. *Clim Dyn* 51:4451–4467. <https://doi.org/10.1007/s00382-017-3926-0>
- Deser C, Phillips AS (2006) Simulation of the 1976/77 climate transition over the North Pacific: Sensitivity to tropical forcing. *J Clim* 19:6170–6180
- Deser C, Phillips AS, Hurrell JW (2004) Pacific interdecadal climate variability: linkages between the tropics and the North Pacific during boreal winter since 1900. *J Clim* 17:3109–3124
- Di Lorenzo E, Cobb KM, Furtado JC, Schneider N, Anderson BT, Bracco A, Alexander MA, Vimont DJ (2010) Central Pacific El Niño and decadal climate change in the North Pacific Ocean. *Nat Geosci* 3:762–765. <https://doi.org/10.1038/NGEO984>
- Di Lorenzo E, Liguori G, Schneider N, Furtado JC, Anderson BT, Alexander MA (2015) ENSO and meridional modes: a null hypothesis for Pacific climate variability. *Geophys Res Lett* 42:9440–9448. <https://doi.org/10.1002/2015GL066281>

- Dong B, Dai A (2015) The influence of the interdecadal Pacific oscillation on temperature and precipitation over the globe. *Clim Dyn*. <https://doi.org/10.1007/s00382-015-2500-x>
- Dong B, Dai A, Vuille M, Timm OE (2018) Asymmetric modulation of ENSO teleconnections by the Interdecadal Pacific Oscillation. *J Clim* 31(18):7337–7361. <https://doi.org/10.1175/JCLI-D-17-0663.1>
- Du Y, Yang L, Xie S-P (2011) Tropical Indian Ocean influence on Northwest Pacific tropical cyclones in summer following strong El Niño. *J Clim* 24:315–322
- England MH, McGregor S, Spence P, Meehl GA, Timmermann A, Cai W, Gupta AS, McPhaden MJ, Purich A, Santoso A (2014) Recent intensification of wind-driven circulation in the Pacific and the on-going warming hiatus. *Nat Clim Change* 4:222–227
- Fan H, Huang H (2008) Response of coastal marine eco-environment to river fluxes into the sea: a case study of the Huanghe (Yellow) River mouth and adjacent waters. *Mar Environ Res* 65:378–387
- Fan L, Shin S-I, Liu Q, Liu Z (2013) Relative importance of tropical SST anomalies in forcing East Asian summer monsoon circulation. *Geophys Res Lett* 40:2471–2477. <https://doi.org/10.1002/grl.50494>
- Gao S, Li X (2008) Responses of tropical deep convective precipitation systems and their associated convective and stratiform regions to the large-scale forcing. *Q J R Meteorol Soc* 134(637):2127–2141. <https://doi.org/10.1002/qj.331>
- Gao G, Marin M, Feng M, Yin B (2020) Drivers of marine heatwaves in the East China Sea and the south Yellow Sea in three consecutive summers during 2016–2018. *J Geophys Res Oceans* 125:e2020JC016518
- Gu D, Philander GH (1997) Interdecadal climate fluctuations that depend on exchanges between the tropics and extratropics. *Science* 275:805–807
- Guan C, McPhaden MJ (2016) Ocean processes affecting the twenty-first-century shift in ENSO SST variability. *J Clim* 29:6861–6879. <https://doi.org/10.1175/JCLI-D-15-0870.1>
- Ha K-J, Heo K-Y, Lee S-S, Yun K-S, Jhun J-G (2012) Variability in the East Asian Monsoon: a review. *Meteorol Appl* 19:200–215. <https://doi.org/10.1002/met.1320>
- Ha K-J, Nam S, Jeong J-Y, Moon I-J, Lee M, Yun J, Jang CJ, Kim YS, Byun DS, Heo K-Y, Shim J-S (2019) Observations utilizing Korea ocean research stations and their applications for process studies. *B Am Meteorol Soc*. <https://doi.org/10.1175/BAMS-D-18-0305.1>
- Ham YG, Kug JS, Park JY, Jin FF (2013) Sea surface temperature in the north tropical Atlantic as a trigger for El Niño/Southern Oscillation events. *Nat Geosci* 6(2):112–116. <https://doi.org/10.1038/ngeo1686>
- He J, Lin H, Wu Z (2011) Another look at influences of the Madden-Julian Oscillation on the wintertime East Asian weather. *J Geophys Res* 111:D03109. <https://doi.org/10.1029/2010JD014787>
- Hersbach H, Bell B, Berrisford P et al (2020) The ERA5 global reanalysis. *Q J R Meteorol Soc*. <https://doi.org/10.1002/qj.3803>
- Hu Z-Z, Kumar A, Huang B, Zhu J, Ren H-L (2017) Interdecadal variations of ENSO around 1999/2000. *J Meterol Res* 31:73–81. <https://doi.org/10.1007/s13351-017-6074-x>
- Imada Y, Tatebe H, Watanabe M, Ishii M, Kimoto M (2016) South Pacific influence on the termination of El Niño in 2014. *Sci Rep* 6:30341. <https://doi.org/10.1038/srep30341>
- Jo H-S, Yeh S-W, Lee S-K (2015) Changes in the relationship in the SST variability between the tropical Pacific and the North Pacific across the 1998/1999 regime shift. *Geophys Res Lett* 42:7171–7178. <https://doi.org/10.1002/2015GL065049>
- Kim YS, Jang CJ, Yeh S-W (2018a) Recent surface cooling in the Yellow and East China Seas and the associated North Pacific regime shift. *Cont Shelf Res* 156:43–54
- Kim YS, Jang CJ, Jeong JY, Shim JS (2018b) Daily to seasonal variability of the mixed layer depth in the central Yellow Sea: effects of atmospheric forcing. *J Coast Res* SI85:576–580. <https://doi.org/10.2112/SI85-116.1>
- Kim YS, Jang CJ, Noh JH, Kim KT, Kwon JI, Min Y, Jeong J, Lee J, Min IK, Shim JS, Byun DS (2019) A Yellow Sea monitoring platform and its scientific applications. *Front Mar Sci* 6:601. <https://doi.org/10.3389/fmars.2019.00601>
- Kim G-U, Lee K, Lee J, Jeong J-Y, Lee M, Jang CJ, Ha K-J, Nam S, Noh JH, Kim YS (2022) Record-breaking slow temperature evolution of spring water during 2020 and its impacts on spring bloom in the Yellow Sea. *Front Mar Sci* 9:824361. <https://doi.org/10.3389/fmars.2022.824361>
- Kohyama T, Hartmann DL (2017) Nonlinear ENSO warming suppression (NEWS). 30:4227–4251. <https://doi.org/10.1175/JCLI-D-16-0541.1>
- Kohyama T, Hartmann DL, Battisti DS (2017) La Niña-like mean-state response to global warming and potential oceanic roles. *J Clim* 30:4207–4225. <https://doi.org/10.1175/JCLI-D-16-0441.1>
- Larson SM, Pegion KV, Kirtman BP (2018) The South Pacific meridional mode as a thermally driven source of ENSO amplitude modulation and uncertainty. *J Clim* 31:5127–5145. <https://doi.org/10.1175/JCLI-D-17-0722.1>
- Lau N-C, Nath MJ (1996) The role of the atmospheric bridge in linking tropical Pacific ENSO events to extratropical SST anomalies. *J Clim* 9:2036–2057
- Li X, Hu Z-Z, Becker E (2019) On the westward shift of tropical Pacific climate variability since 2000. *Clim Dyn* 53:2905–2918. <https://doi.org/10.1007/s00382-019-04666-8>
- Liao E, Lu W, Yan X-H, Jiang Y, Kidwell A (2015) The coastal ocean response to the global warming acceleration and hiatus. *Sci Rep* 5:16630. <https://doi.org/10.1038/srep16630>
- Lie HJ, Cho CH (2016) Seasonal circulation patterns of the Yellow and East China Seas derived from satellite-tracked drifter trajectories and hydrographic observations. *Prog Oceanogr* 146:121–141
- Lie HJ, Cho CH, Lee JH, Lee S (2003) Structure and eastward extension of the Changjiang River plume in the East China Sea. *J Geophys Res: Oceans* 108(C3)
- Liguori G, Di Lorenzo E (2018) Meridional modes and increasing Pacific decadal variability under anthropogenic forcing. *Geophys Res Lett*. <https://doi.org/10.1002/2017GL076548>
- Liguori G, Di Lorenzo E (2019) Separating the North and South Pacific Meridional Modes contributions to ENSO and tropical decadal variability. *Geophys Res Lett* 46:906–915. <https://doi.org/10.1029/2018GL080320>
- Lima FP, WetHEY DS (2012) Three decades of high-resolution coastal sea surface temperatures reveal more than warming. *Nat Commun* 3:704. <https://doi.org/10.1038/ncomms1713>
- Liu N, Wang H, Ling T, Feng L (2013) The influence of ENSO on sea surface temperature variations in the China seas. *Acta Oceanol Sin* 32(9):21–29. <https://doi.org/10.1007/s13131-013-0348-7>
- Liu T, Li J, Li Y, Zhao S, Zheng F, Zheng J (2018) Influence of the May Southern annular mode on the South China Sea summer monsoon. *Clim Dyn* 51:4095–4107. <https://doi.org/10.1007/s00382-017-3753-3>
- McGregor S, Timmermann A, Stuecker MF, England MH, Merrifield M, Jin F-F, Chikamoto Y (2014) Recent Walker circulation strengthening and Pacific cooling amplified by Atlantic warming. *Nat Clim Change* 4:888–892. <https://doi.org/10.1038/nclimate2330>
- McPhaden MJ (2012) A 21st century shift in the relationship between ENSO SST and warm water volume anomalies. *Geophys Res Lett* 39:L09706. <https://doi.org/10.1029/2012GL051826>
- Min Q, Su J, Zhang R (2017) Impact of the South and North Pacific meridional modes on the El Niño-Southern Oscillation:

- Observational analysis and comparison. *J Clim* 30:1705–1720. <https://doi.org/10.1175/JCLI-D-16-0063.1>
- Newman M, Alexander MA, Ault TR, Cobb KM, Deser C, Di Lorenzo E, Mantua NJ, Miller AJ, Minobe S, Nakamura H, Schneider N, Vimont DJ, Phillips AS, Scott JD, Smith CA (2016) The Pacific decadal oscillation, revisited. *J Clim* 29:4399–4427. <https://doi.org/10.1175/JCLI-D-15-0508.1>
- North GR, Bell TL, Cahalan RF, Moeng FJ (1982) Sampling errors in the estimation of empirical orthogonal functions. *Mon Weather Rev* 110(7):699–706
- Okumura YM (2013) Origins of tropical Pacific decadal variability: role of stochastic atmospheric forcing from the South Pacific. *J Clim* 26:9791–9796. <https://doi.org/10.1175/JCLI-D-13-00448.1>
- Okumura YM, Sun T, Wu X (2017) Asymmetric modulation of El Niño and La Niña and the linkage to tropical Pacific decadal variability. *J Clim* 30:4705–4730. <https://doi.org/10.1175/JCLI-D-16-0680.1>
- Overland J, Rodionov S, Minobe S, Bond N (2008) North Pacific regime shifts: definitions, issues and recent transitions. *Prog Oceanogr* 77:92–102. <https://doi.org/10.1016/j.pocean.2008.03.016>
- Park W-S, Oh I-S (2000) Interannual and interdecadal variations of sea surface temperature in the East Asian Marginal Seas. *Prog Oceanogr* 47:191–204
- Park T, Jang CJ, Jungclaus JH, Haak H, Park W, Oh I-S (2011) Effects of the Changjiang river discharge on sea surface warming in the Yellow and East China Seas in summer. *Cont Shelf Res* 31:15–22. <https://doi.org/10.1016/j.csr.2010.10.012.1>
- Park J-H, Yeo D-E, Lee KJ, Lee H, Lee S-W, Noh S et al (2019) Rapid decay of slowly moving Typhoon Soulik (2018) due to interactions with the strongly stratified northern East China Sea. *Geophys Res Lett*. <https://doi.org/10.1029/2019GL086274>
- Rayner NA, Parker DE, Horton EB, Folland CK, Alexander LV, Rowell DP, Kent EC, Kaplan A (2003) Global analyses of sea surface temperature, sea ice, and night marine air temperature since the late nineteenth century. *J Geophys Res* 108(D14):4407. <https://doi.org/10.1029/2002JD002670>
- Reynolds RW, Chelton DB (2010) Comparisons of daily sea surface temperature analyses for 2007–08. *J Clim* 23:3545–3562
- Reynolds RW, Smith TM, Liu C, Chelton DB, Casey KS, Schlax MG (2007) Daily high-resolution-blended analyses for sea surface temperature. *J Clim* 20:5473–5496. <https://doi.org/10.1175/2007JCLI1824.1>
- Sarthi PP, Kumar P (2022) Intraseasonal variability and possible causes of large-scale and convective precipitations over the Gangetic plain of India. *Theor Appl Climatol* 147:1453–1469. <https://doi.org/10.1007/s00704-021-03881-w>
- Stuecker MF (2018) Revisiting the Pacific meridional mode. *Sci Rep* 8:3216. <https://doi.org/10.1038/s41598-018-21537-0>
- Tak YJ, Cho YK, Seo GH, Choi BJ (2016) Evolution of wind-driven flows in the Yellow Sea during winter. *J Geophys Res Oceans* 121(3):1970–1983
- Tonizzzo T (2010) Climate variability in the south-eastern tropical Pacific and its relation with ENSO: a GCM study. *Clim Dyn* 34:1093–1114
- Trenberth KE, Branstator GW, Karoly D, Kumar A, Lau N-C, Ropelewski C (1998) Progress during TOGA in understanding and modeling global teleconnections associated with tropical sea surface temperatures. *J Geophys Res* 103(C7):14291–14324
- Vimont DJ, Wallace JM, Battisti DS (2003) The seasonal footprinting mechanism in the Pacific: implications for ENSO. *J Clim* 16:2668–2675
- Wang F (2010) Subtropical dipole mode in the Southern Hemisphere: a global view. *Geophys Res Lett* 37:L10702. <https://doi.org/10.1029/2010GL042750>
- Wang J, Oey L-Y (2014) Inter-annual and decadal fluctuations of the Kuroshio in East China Sea and connection with surface fluxes of momentum and heat. *Geophys Res Lett* 41:8538–8546. <https://doi.org/10.1002/2014GL062118>
- Wang B, Zhou X (2008) Climate variation and prediction of rapid intensification in tropical cyclones in the western North Pacific. *Meteorol Atmos Phys* 99:1–16. <https://doi.org/10.1007/s00703-006-0238-z>
- Wang B, Wu R, Fu X (2000) Pacific-East Asian teleconnection: how does ENSO affect East Asian climate? *J Clim* 13:1517–1536
- Wang B, Xiang B, Lee J-Y (2013) Subtropical High predictability establishes a promising way for monsoon and tropical storm predictions. *P Natl Acad Sci USA* 110(8):2718–2722. <https://doi.org/10.1073/pnas.1214626110>
- Wu Z, Dou J, Lin H (2015) Potential influence of the November–December Southern Hemisphere annular mode on the East Asian winter precipitation: a new mechanism. *Clim Dyn* 44:1215–1226. <https://doi.org/10.1007/s00382-014-2241-2>
- Wu R, Lin J, Li B (2016) Spatial and temporal variability of sea surface temperature in eastern marginal seas of China. *Adv Meteorol* 2015:3820720. <https://doi.org/10.1155/2016/3820720>
- Xiang B, Wang B, Yu W, Xu S (2013) How can anomalous western North Pacific Subtropical High intensify in late summer? *Geophys Res Lett* 40:2349–2354. <https://doi.org/10.1002/grl.50431>
- Xie P, Arkin PA (1997) Global precipitation: A 17-YEAR monthly analysis based on gauge observations, satellite estimates, and numerical model outputs. *Bull Am Meteorol Soc* 78:2539–2558
- Xie S-P, Kosaka Yu, Du Y, Hu K, Chowdary JS, Huang G (2016) Indo-western Pacific Ocean capacitor and coherent climate anomalies in post-ENSO summer: a review. *Adv Atmos Sci* 33(4):411–432. <https://doi.org/10.1007/s00376-015-5192-6>
- Yang F, Lau K-M (2004) Trend and variability of China precipitation in spring and summer: linkage to sea-surface temperatures. *Int J Climatol* 24:1625–1644. <https://doi.org/10.1002/joc.1094>
- Yang Y-M, Park J-H, An S-I, Wang B, Luo X (2021) Mean sea surface temperature changes influence ENSO-related precipitation changes in the mid-latitudes. *Nat Commun* 12:1495
- Yeh S-W, Kim C-H (2010) Recent warming in the Yellow/East China Sea during winter and the associated atmospheric circulation. *Cont Shelf Res* 30:1428–1434
- Yeh S-W, Kug J-S, Dewitte B, Kwon M-H, Kirtman B, Jin F-F (2009) El Niño in a changing climate. *Nature* 461:511–514. <https://doi.org/10.1038/nature08316>
- Yeh S-W, Wang X, Wang C, Dewitte B (2015) On the relationship between the North Pacific climate variability and the central Pacific El Niño. *J Clim* 28:663–677. <https://doi.org/10.1175/JCLI-D-14-00137.1>
- Yeo S-R, Kim K-Y (2014) Global warming, low-frequency variability, and biennial oscillation: an attempt to understand the physical mechanisms driving major ENSO events. *Clim Dyn* 43:771–786. <https://doi.org/10.1007/s00382-013-1862-1>
- Yeo S-R, Kim K-Y, Yeh S-W, Kim W-M (2012) Decadal changes in the relationship between the tropical Pacific and the North Pacific. *J Geophys Res* 117:D15102. <https://doi.org/10.1029/2012JD017775>
- Yim S-Y, Jhun J-G, Yeh S-W (2008) Decadal change in the relationship between east Asian–western North Pacific summer monsoons and ENSO in the mid-1990s. *Geophys Res Lett* 35:L20711. <https://doi.org/10.1029/2008GL035751>
- You Y, Furtado JC (2017) The role of South Pacific atmospheric variability in the development of different types of ENSO. *Geophys Res Lett* 44:7438–7446. <https://doi.org/10.1002/2017GL073475>
- Yun K-S, Timmermann A, Stuecker MF (2021) Synchronized spatial shifts of Hadley and Walker circulations. *Earth Syst Dynam* 12:121–132. <https://doi.org/10.5194/esd-12-121-2021>
- Zhang L, Wu L, Lin X, Wu D (2010) Modes and mechanisms of sea surface temperature low-frequency variations over the coastal China seas. *J Geophys Res* 115:C08031. <https://doi.org/10.1029/2009JC006025>

- Zhang H, Clement A, Di Nezio P (2014a) The South Pacific meridional mode: A Mechanism for ENSO-like variability. *J Clim* 27:769–783. <https://doi.org/10.1175/JCLI-D-13-00082.1>
- Zhang H, Deser C, Clement A, Tomas R (2014b) Equatorial signatures of the Pacific Meridional Modes: dependence on mean climate state. *Geophys Res Lett* 41:568–574. <https://doi.org/10.1002/2013GL058842>
- Zhang Y, Yu S, Amaya DJ, Kosaka Y, Larson SM, Wang X, Yang J-C, Stuecker MF, Xie S-P, Miller AJ, Lin X (2021) Pacific meridional modes without equatorial Pacific influence. *J Clim* 34(13):5285–5301. <https://doi.org/10.1175/JCLI-D-20-0573.1>

Publisher's Note Springer Nature remains neutral with regard to jurisdictional claims in published maps and institutional affiliations.

Springer Nature or its licensor holds exclusive rights to this article under a publishing agreement with the author(s) or other rightsholder(s); author self-archiving of the accepted manuscript version of this article is solely governed by the terms of such publishing agreement and applicable law.